Politecnico di Torino

Politecnico di Torino

Master Degree course in Land and Environmental Engineering, Climate Change

Academic Year 2024-2025

Graduating Session

October 2025

Changes in climate extremes in small Pacific Islands from km-scale model simulations

Supervisor:

Prof. Jost-Diedrich Graf Von Hardenberg

Candidate:

Tiziana Tessadri 322201

Co-Supervisor:

Andrea Vito Vacca

Abstract

Pacific Island Countries and Territories (PICTs) are among the most vulnerable regions to climate change due to their small land area, low elevation, high population density, and fragile economies and ecosystems. However, the extent to which climate change will alter the frequency and intensity of extreme events in these territories remains uncertain. This uncertainty arises primarily from the coarse spatial resolution of current-generation general circulation models (GCMs), which are unable to adequately capture the fine-scale morphological and geographical features of the islands. To address this critical knowledge gap, this thesis analyses for the first time kilometer-scale climate simulations from the Destination Earth (DE) Project using the ICON climate model.

The high-resolution ICON model (5 km) is compared with two reanalysis datasets, ERA5 (25 km) and BARRA (12 km), to assess the influence of model resolution on the climatology of daily precipitation, daily maximum and minimum temperatures, and selected climate extreme indices (ETCCDI) for 1990–2019. The study area is divided into three domains, land (islands), halo (ocean adjacent to islands), and sea (open ocean). Results show that the three domains exhibit distinct distributions and trends, with higher-resolution data providing a better representation of small-scale climate features. This effect is especially evident in the analysis of ETCCDI indices related extreme temperatures.

The analysis of near-future projections using the ICON model under SSP3-7.0 shows significant warming trends in daily minimum and maximum temperatures. Precipitation exhibits a significant positive signal over both the Fiji Islands and the equatorial regions, with the latter showing an opposite-sign change when comparing the historical and projected periods. ETCCDI indices display consistent but steeper trends compared to the historical period. In order to move from regional to point-scale analysis, we further examine projected changes in three representative cities of the region (1990-2039). The results show clear, statistically significant increases in daily temperature and related extremes, while precipitation exhibits a statistically significant increase only over Suva, located in the Fiji Islands.

These findings highlight the added value of high-resolution climate simulations for small island regions, where climate change information is vital for adaptation.

Contents

List of Figures

List of Tables

1. Introduction

1.1 Climate Patterns in the Pacific Ocean

Climate change represents a major and increasingly visible threat, especially in areas where the economy and people's livelihoods depend almost entirely on the state of the climate. PICTs (Pacific Island Countries and Territories) are among the territories that suffer the most from these conditions, due to both events that have occurred in the region and their exposure and vulnerability (McGree, Herold, et al., 2019).

Situated in the middle of the Pacific Ocean, they are influenced by large-scale climate processes that occur in the Tropical Pacific: El Niño–Southern Oscillation (ENSO), the largest mode of climate variability in the Earth System (S. Chand et al., 2023), is characterized by three phases: El Niño, La Niña, and a neutral phase; the Madden–Julian Oscillation (MJO), which involves deep convective activity that modulates rainfall across the Pacific Island nations (S. Chand et al., 2023); the Pacific Decadal Oscillation (PDO), which affects sea surface temperatures in the central and eastern Pacific (S. Chand et al., 2023). The heterogeneity, complexity, and significance of the selected study area arise from the particular location of the small islands, illustrated in Figures 1.1 and 1.4, where they are highlighted by a red/blue rectangle. In the Pacific Ocean, daily maximum and daily minimum temperatures decrease with increasing distance from the Equator. Maximum temperatures reach up to about 28°C, while minimum temperatures attain their highest values near Australia, at around 25°C (Figure 1.1).

The temperature zonal asymmetry visible in both maps is associated with the so-called cold tongue in the eastern Pacific and the warm pool in the western Pacific. The cold tongue region (Figure 1.2) is characterized by strong interannual fluctuations in sea surface temperature (SST), primarily driven by ENSO (Figure 1.3). This atmosphere-ocean coupled mode of variability arises from the zonal structure of the ocean thermocline: it is much deeper in the west than in the east, creating a pronounced temperature gradient that maintains higher SSTs in the western Pacific (Cai, 2003; Zelle et al., 2004). During the different ENSO phases, the Pacific Ocean responds in distinct ways (Figure 1.3). When El Niño phase develops, the sea surface temperatures (SSTs) become warmer in the eastern tropical Pacific, while negative SST anomalies appear in the western tropical Pacific. Conversely, during the La Niña phase, anomalies of opposite sign occur,

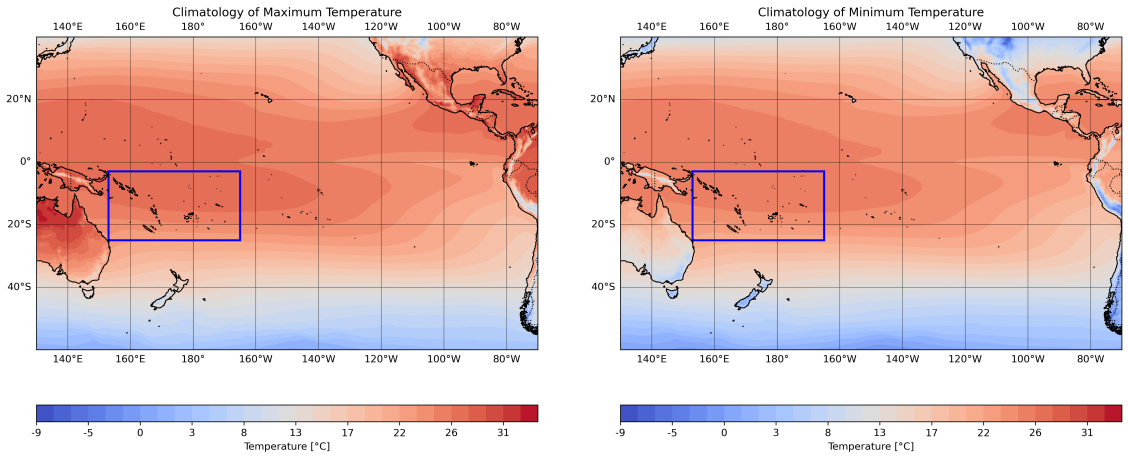

(a) Climatology of Daily Maximum Temperature

(b) Climatology of Daily Minimum Temperature

Figure 1.1: Climatology of Daily maximum and minimum temperatures (1950–2023) over the Pacific Ocean from ERA5 data.

with a decrease in SSTs across much of the Pacific Ocean (S. Chand et al., 2023; Fiedler, 2002).

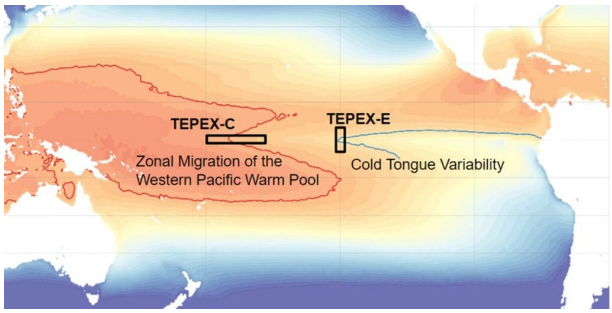

Figure 1.2: Location of the Equatorial Cold Tongue and West Pacific Warm Pool. Source: Climate Program Office, NOAA (2024).

Although the warm pool has a deeper mixed layer, it initially warms faster than the cold tongue because the latter is strongly cooled by upwelling of cold subsurface water. Over time, however, subsurface warming reduces the vertical temperature gradient in the cold tongue

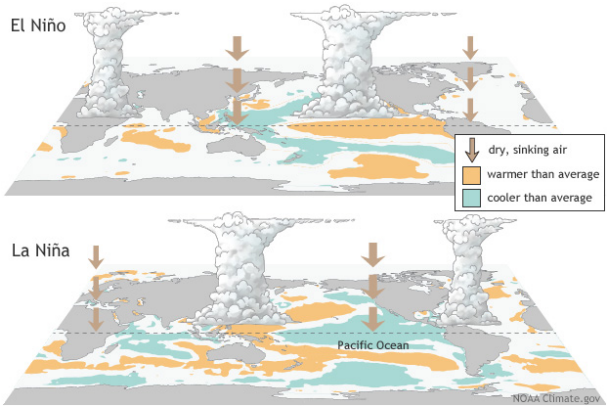

Figure 1.3: Schematic representation of atmospheric dynamics and sea surface temperature anomalies during *El Niño* (top) and *La Niña* (bottom). Orange areas indicate warmer-than-average sea surface temperatures, while blue areas indicate cooler-than-average conditions. Brown arrows represent dry, sinking air. Source: Climate.gov (2021).

region, weakening the cooling effect of upwelling and allowing its surface to warm more rapidly, potentially exceeding the warming of the warm pool (An et al., 2012).

The map in Figure 1.4 shows the climatological distribution of precipitation over the Pacific Ocean and highlights two intense bands of rainfall and deep atmospheric convection that influence the study area. Above is located the Intertropical Convergence Zone (ITCZ), while the diagonal band extending from the equator toward the subtropical South Pacific known as the South Pacific Convergence Zone (SPCZ), which represents a southeastward extension of the ITCZ (Brown et al., 2020).

The ITCZ is a convective region where approximately one-third of the world's total precipitation occurs. Its location can vary over long timescales due to a variety of external forcings, both natural and anthropogenic (Liu et al., 2024). Numerous studies have investigated the Intertropical Convergence Zone (ITCZ) and its position, which significantly influences the climate across many regions. Aumann, Broberg, and Manning (2024) reported a northward shift and narrowing of the Intertropical Convergence Zone (ITCZ) over the past two decades. The article describes how this shift is related to hemispheric imbalances in landmass and energy between the Southern and Northern Hemispheres, causing the southern boundary of the ITCZ to shift northward more rapidly than the northern boundary, thereby narrowing the zone. Studies are investigating how the ITCZ may behave in the coming decades, driven by the effects of climate change. Liu et al.

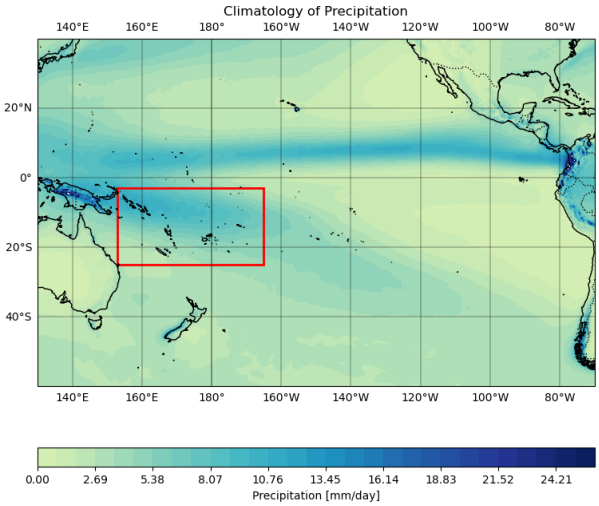

Figure 1.4: Mean daily precipitation over the Pacific Ocean from ERA5 reanalysis data (1940–2025).

(2024) used CO_2-quadrupling simulations to show that an initial rapid northward shift of the ITCZ is expected during the first 20 years, consistent with the findings of Aumann, Broberg, and Manning (2024). However, over a longer timescale, between 100 and 1000 years, a gradual southward shift is projected, attributed to the delayed warming of the Southern Ocean.

The South Pacific Convergence Zone (SPCZ) is the largest rainband in the Southern Hemisphere and plays a crucial role in rainfall across the southwest Pacific Islands, particularly during the austral summer (December–February). It also influences the location and tracks of tropical cyclones, as well as sea-level anomalies (Brown et al., 2020). The SPCZ is modulated by additional climate drivers, including the El Niño–Southern Oscillation (ENSO) and the Madden–Julian Oscillation (MJO) (World Meteorological Organization, 2024), which makes it extremely challenging to predict and to fully understand the complex dynamic processes involved. These drivers also modulate temperatures across the Pacific region. In particular, during El Niño events, islands in the southwest Pacific typically experience drier conditions, while islands near the equator and east of the mean SPCZ position tend to experience wetter conditions. The opposite pattern occurs during La Niña events, as shown in Figure 1.3 (Brown et al., 2020).

The movement and intensity of the SPCZ have been monitored, highlightening a southern positioning in the first decades of the 1900s, likely due to a cooler North Atlantic, stronger Pacific

trade winds, a cool-phase Pacific Decadal Oscillation (PDO) and limited El Niño activity (Linsley et al., 2017). The displacement and intensity of the SPCZ are influenced by various factors, including interactions between the tropical and extratropical atmosphere, which are themselves shaped by underlying sea surface temperature gradients (Brown et al., 2020). Historical data have been analyzed to identify pattern changes related to anthropogenic factors, but no significant results have emerged due to the large natural multi-decadal variability of the SPCZ (Brown et al., 2020). Future projections of the South Pacific Convergence Zone (SPCZ) indicate a likely northeastward shift due to both thermodynamic processes ('wet-gets-wetter') and dynamic processes ('warmest-gets-wetter') (Widlansky et al., 2013). Increased equatorial warming enhances convection near the Equator, reducing rainfall in the SPCZ's southeastern branch. Multi-model projections suggest that under moderate warming (1–2,°C), rainfall may decrease by 6% (±20%), mainly due to dry air advection suppressing convection. In contrast, under high warming scenarios (> 3,°C), precipitation could increase as the atmosphere retains more moisture despite drying dynamics. Other studies, such as the one led by Narsey et al. (2022), analyzing projections under RCP8.5 and SSP5-8.5 scenarios, show that multi-model means suggest three possible outcomes for the SPCZ: a northward shift, a southward shift, or no significant change. This highlights the high level of uncertainty surrounding the future behavior of the SPCZ.

1.2 Pacific Island Countries and Territories

The area highlighted in Figure 1.4 is part of the Pacific Island Countries and Territories (PICTs), comprising three distinct groups: Micronesia, Polynesia, and Melanesia (Figure 1.5). These include independent states, associated states, integral parts of non-Pacific Island countries, and dependent territories for an amount of 28 countries (Iese et al., 2021).

Thousands of islands are present in this region, exhibiting wide variations in climatic conditions (Goldberg, 2018). In particular, the selected area includes the following island groups: the Solomon Islands, New Caledonia, Tuvalu, Samoa, the Cook Islands, Tonga, Vanuatu, and Wallis and Futuna. These islands have an average area of less than 100 km^2 (Nunn et al., 2016), and their sizes vary widely: from larger islands with mountains and rivers, such as Fiji, to atolls whose highest point is only 5 m above sea level, such as Tuvalu (Iese et al., 2021). These islands have a tropical climate characterized by minimal seasonal temperature variation (NOAA National Climatic Data Center, 2012), with mean annual temperatures typically ranging between 26°C and 28°C, and a difference of only about 0.5°C between the warmest and coolest months. On

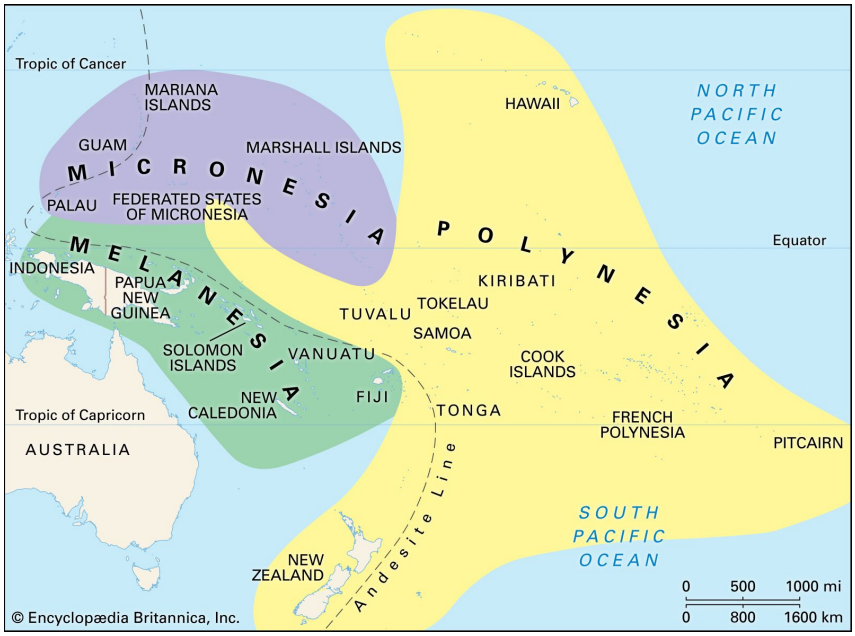

Figure 1.5: Culture areas of the Pacific Islands. Source: Encyclopædia Britannica, Inc., *Culture areas of the Pacific Islands* [Image], Encyclopædia Britannica. `https://cdn.britannica.com/57/126157-050-7F6512BB/Culture-areas-Pacific-Islands.jpg`, accessed July 4, 2025.

a regional scale, increases in both maximum and minimum temperatures have been observed, along with a rise in warm extremes, which does not appear to be linked to the high variability of the area (McGree, Herold, et al., 2019).

The region is characterized by distinct wet and dry periods, with the dry season typically spanning from May to October, and the wet season occurring from November to April, in line with the Southern Hemisphere's seasonal cycle (Pacific-Australia Climate Change Science and Adaptation Planning Program, 2013). Due to the movement of the South Pacific Convergence Zone (SPCZ), which influences the tropical cyclone seasons, approximately 20% of the total precipitation in the South Pacific region is attributed to these events (Fernández-Duque et al., 2024).

In recent decades, changes in precipitation and related indices have been assessed, but the analysis remains complex. While droughts have increased in length in recent years, projections for the coming decades suggest an increase in mean annual precipitation, accompanied by shorter drought periods. This indicates a likely rise in the frequency of extreme events (McGree, Herold,

et al., 2019; Iese et al., 2021).

1.2.1 Socio-Economic Scenario of PICTs

The population of the PICTs exceeds 14 million people in 2025 and is projected to increase further in the future[1], they are largely dependent on agriculture and on water sourced from precipitation events or shallow groundwater (Iese et al., 2021). People on the islands primarily work in the fishing and farming sectors, but the balance between populations and natural resources is increasingly threatened by the shift from predominantly agricultural to urban societies, as well as by climate change and its associated extreme events (Shah, Moroca, and Bhat, 2018). Another major source of economic income for these islands is tourism, which significantly contributes to the development goals of these nations, particularly in terms of infrastructure and employment. However, this sector is now under threat due to the lingering impacts of the COVID-19 pandemic and the increasing frequency of extreme weather events (Wolf et al., 2021). The health sector is another area being heavily impacted by rising temperatures and variations in precipitation patterns. A significant proportion of hospitals, many located within 500 meters of the coast, are at risk due to sea level rise (Taylor, 2021). Additionally, new diseases are spreading as a result of increasing temperatures and humidity, while food security is becoming increasingly threatened. Health risks associated with flooding and heatwaves are also on the rise (McIver et al., 2016).

Island societies are not only defined by their physical geography but also by their cultural heritage, indigenous knowledge, health, and social cohesion. These dimensions, often referred to as non-economic aspects of loss and damage, are critical to understanding the full impact of climate-related events (McNamara et al., 2021).

In the territory, diverse ecosystems such as tropical rainforests, grasslands, and coral reefs coexist (Palanivel and Shah, 2021). Climate change and human development threat the unique biodiversity of both terrestrial and marine ecosystems, including coral reefs, leading to the loss of numerous plant and animal species on land and in the ocean (Jupiter, Mangubhai, and Kingsford, 2014).

The threat posed by climate change is more present than ever, and the PICTs are on high alert. From the World Meteorological Organization (2024) annual report "over 25 million people were directly affected [...], and they caused a total economic damage of close to US$ 4.4 billion." In Figure 1.7, the damages caused and their associated event types are reported.

[1] Pacific Community (SPC), *Homepage*, accessed July 20, 2025, `https://www.spc.int/`.

Figure 1.6: Typology of NELD in the Pacific Islands region (© Copyright PresentationGO.com). Source: McNamara et al. (2021)

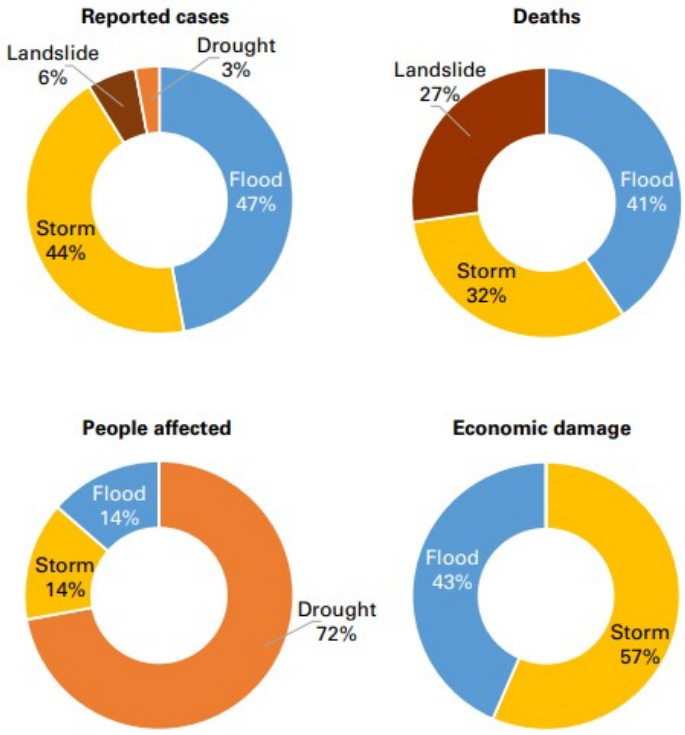

Figure 1.7: Overview of 2023 disasters in the South-West Pacific region. *Note: The economic damages resulting from some disasters are not presented in the diagram due to data unavailability. Only cases reported in EM-DAT are considered in the diagram.*
Source: World Meteorological Organization (2024) calculations based on EM-DAT data, accessed on 23 July 2025.

In response to increasing climate-related risks, Australia and Tuvalu, a small island nation in the central Pacific with a population of around 11,000, signed a groundbreaking agreement in 2023 known as the *Australia–Tuvalu Falepili Union Treaty*. This treaty addresses climate change adaptation, migration, and security, and allows the people of Tuvalu to move to, live, and work in Australia (Barnett et al., 2025).

1.2.2 Evidence of Changes in Climate Extremes

The increase in weather-related natural catastrophes has been recognized worldwide since 1980 (Heim Jr, 2015). In the South West Pacific region, the main hazardous events are tropical

cyclones, floods, and droughts (Kuleshov et al., 2014), as well as heat waves (Lo et al., 2024). While La Niña and El Niño normally influence these events, recent reports describe climate extremes—such as droughts or cyclones—that occur outside their typical patterns (World Meteorological Organization, 2024). In 2019, five Pacific Island countries were ranked among the top 20 in the World Risk Index for exposure to extreme natural events, with Vanuatu and Tonga occupying the first and third positions, respectively (Bündnis Entwicklung Hilft and Institute for International Law of Peace and Armed Conflict, 2019).

In terms of tropical cyclones, whose season in the Southern Hemisphere spans from November to April, the number of events recorded at the end of 2024 was below average (World Meteorological Organization, 2025a). In the study by Deo et al. (2021), future projections indicate a possible decrease in the frequency of such events, accompanied by an increase in their intensity. In 2023, Fiji experienced the highest November 24-hour rainfall, reaching 178 mm, followed by the arrival of Severe Tropical Cyclone *Mal* (World Meteorological Organization, 2024). Considering heavy precipitation and flooding, Fiji, particularly the island of Viti Levu, experienced significant flooding in late December of 2024, with monthly rainfall exceeding two to three times the normal levels (World Meteorological Organization, 2025a).

Regarding droughts, their impact on Pacific Islands varies significantly depending on geographic location, which is influenced by ENSO variability as well as the positions of the Intertropical Convergence Zone (ITCZ) and the South Pacific Convergence Zone (SPCZ) (Iese et al., 2021). Records from 2023 show that several Pacific Islands experienced a second consecutive year of drier-than-average conditions. This was largely driven by the transition from La Niña to El Niño, yet precipitation levels remained below normal throughout the year (World Meteorological Organization, 2024).

Heat waves are also important threats for these territories, which expose humans to high risks such as dehydration, heat stroke, and cardiovascular and respiratory problems, potentially leading to death (Lo et al., 2024).

The objective of this thesis is to evaluate changes in daily temperature and precipitation extremes in the Pacific Island Countries and Territories, regions that are poorly represented in global climate models due to their coarse spatial resolution (Doorga, 2022; Doblas-Reyes et al., 2025). For the first time, this study overcomes such limitations by employing a high-resolution climate model with a 5 km spatial resolution from the Destination Earth project simulations (DestinE Project, 2025), enabling a more accurate analysis of these territories and how climate extremes have evolved, and are projected to evolve, under anthropogenic influence. To assess the benefits of improved spatial resolution, daily maximum and minimum temperature and precipitation

data from ICON, the model considered in the Climate Change Adaptation Digital Twin of the Destination Earth project, are compared with two reanalysis datasets: ERA5 (25 km resolution) and BARRA (12 km resolution). The second step involves analyzing future projections under the SSP3-7.0 scenario to evaluate the evolution of climate extremes in the study area.

2. Data and Model

2.1 Introduction

The data used in this thesis originate from three different datasets: the ERA5 reanalysis (ECMWF, 2021), the BARRA reanalysis (Australian Bureau of Meteorology, 2024), and a high-resolution climate simulation realized with the ICON climate model (Deutscher Wetterdienst, 2024) in the context of the Destination Earth Project (DestinE Project, 2025). The historical data span the period from 1990 to 2019, while future projections provided by the ICON simulation span the period from 2020 to 2039. These three datasets, described in detail in the following sections, cover the same geographical region, but with progressively higher spatial resolution. The variables of interest are the precipitation rate, and the daily maximum and minimum temperatures. These three variables were selected because they are highly affected by global warming (Cruz-González et al., 2025) and, in turn, have a direct impact on livelihoods (World Meteorological Organization, 2025b). Based on these variables, selected indices from the Expert Team on Climate Change Detection and Indices (ETCCDI) are calculated and analyzed.

2.2 ERA5 Reanalysis

ERA5 is a comprehensive reanalysis dataset that spans from 1940 to five days before the present, and represents the fifth-generation reanalysis produced by the European Centre for Medium-Range Weather Forecasts (ECMWF) (ECMWF, 2021). ECMWF is an independent intergovernmental organisation supported by 35 member and cooperating states (European Centre for Medium-Range Weather Forecasts (ECMWF), 2025). ERA5 data combine real observations from meteorological stations with model outputs. In this system, the atmospheric model is coupled with a land surface model and a wave model, which together contribute to improving the overall data quality. The data, obtained from the Copernicus Climate Data Store (Hersbach et al., 2023), are gridded on a regular 0.25-degree latitude-longitude grid (around 25 km), with an hourly temporal resolution (Copernicus Climate Change Service, 2017). Table 2.1 reports the

variables analysed in this work and their description[1].

Table 2.1: Description of ERA5 variables used in the analysis

Full Name	**Units**	**Variable Name**	**Detailed Definition**
Total precipitation	m/h	`tp`	This parameter is the accumulated liquid and frozen water—comprising rain and snow—that falls on the Earth's surface.
Maximum temperature at 2 m since previous post-processing	K	`mx2t`	This parameter is the highest daily air temperature at 2 m above the surface of land, sea or inland waters.
Minimum temperature at 2 m since previous post-processing	K	`mn2t`	This parameter is the lowest daily air temperature at 2 m above the surface of land, sea or inland waters.

2.3 BARRA

The Bureau of Meteorology High-Resolution Regional Reanalysis for Australia (BARRA) is a high-resolution, multi-decadal regional atmospheric reanalysis. It is a national mesoscale (12 km resolution) reanalysis over Australia and the surrounding regions (Australian Bureau of Meteorology, 2024). BARRA is generated by executing a regional weather forecast model that is driven by global reanalysis data at its boundaries and refined through data assimilation to better match observations (Su et al., 2019). The variables used are downloaded from Bureau of Meteorology (2021) and they are described in Table 2.2 [2].

[1](ECMWF, 2023)

[2](Bureau of Meteorology, 2019)

Table 2.2: Key BARRA parameters: accumulated precipitation and maximum/minimum screen-level temperature.

Full name	**Units**	**Variable name**	**Detailed Description**
Total precipitation amount	$\mathrm{kg\,m^{-2}\,(6h^{-1})}$	`accum_prcp`	Total precipitation amount at the surface in $\mathrm{kg\,m^{-2}}$ in 6 hours. This is the sum of the large-scale and convective rainfall and snowfall at the surface.
Temperature at 1.5 m (Maximum)	K	`max_temp_scrn`	Estimate of atmospheric maximum temperature at 1.5 m. Calculated by integrating the similarity equations from the surface to 1.5 m.
Temperature at 1.5 m (Minimum)	K	`min_temp_scrn`	Estimate of atmospheric minimum temperature at 1.5 m. Calculated by integrating the similarity equations from the surface to 1.5 m.

2.4 Destination Earth

Destination Earth (DestinE Project, 2025) is a European initiative aimed at developing a highly accurate digital replica of the Earth by 2030. The project involves several organizations, in particular the European Centre for Medium-Range Weather Forecasts (ECMWF), the European Space Agency (ESA), and the European Organisation for the Exploitation of Meteorological Satellites (EUMETSAT) (DestinE Project, 2025). The key objectives of DestinE, particularly for the Climate Change Adaptation Digital Twin (*Climate Change Adaptation Digital Twin* 2024) within the DestinE project, include improving spatial resolution to reduce approximation errors and better capture process interactions; enhancing the integration of physical and societal system models, such as the full incorporation of hydrological models; and providing a new interface

for accessing and exploring data and information (Hoffmann et al., 2023). These efforts aim to improve upon existing initiatives, such as CMIP and CORDEX, by merging them with climate adaptation goals (Doblas-Reyes et al., 2025).

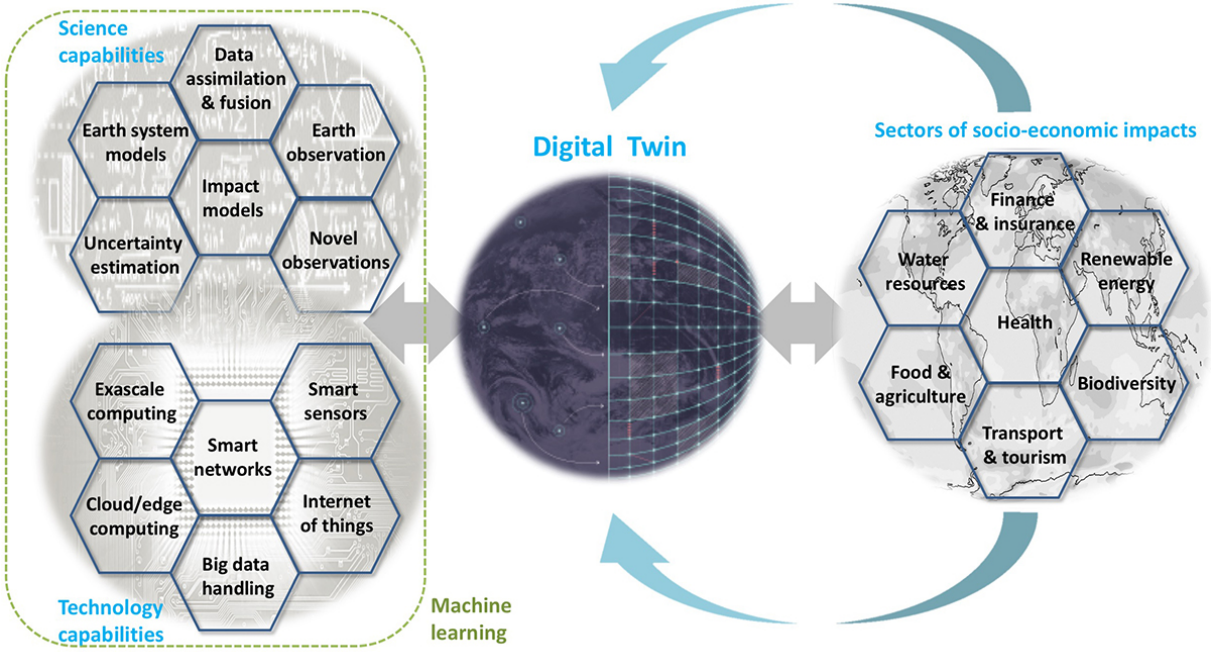

Figure 2.1: Forecasting process chain from observations to applications. Source: Bauer (2022).

The Climate DT provides hourly temporal resolution and kilometer-scale spatial resolution (between 5 and 10 km), making it a highly useful tool for adaptation decision-making and for evaluating existing climate challenges (Doblas-Reyes et al., 2025). High-resolution climate simulations pose significant challenges in terms of memory usage. To address this issue, the Climate DT has been integrated with a Python-based tool called `AQUA` (Application for QUality Assessment), providing a unified end-to-end workflow. Together, this system enables real-time monitoring, systematic comparisons, and quality control of ongoing simulations (Nurisso et al., 2025).

So far, three models have been run as part of the experiments: IFS-NEMO, IFS-FESOM and ICON. In this study, the ICON model is used.

2.4.1 ICON

ICON stands for ICOsahedral Nonhydrostatic and refers to a unified modeling framework for global numerical weather prediction and climate simulation. It solves the full three-dimensional, non-hydrostatic, and compressible Navier–Stokes equations on an icosahedral grid. This approach enables continuous and consistent predictions across a wide range of spatial scales, from local to global (Deutscher Wetterdienst, 2024). For the historical part, ICON uses the R2B9/8 grid configuration, which involves dividing each triangle edge into two parts and connecting the resulting edge midpoints. This process is repeated through 9 successive edge bisections, with new connections formed after each bisection to refine the grid structure (Grundner et al., 2022).

For the historical simulation, the focus is on the recent past, starting from 1990. These past simulations are used to evaluate the model performance before applying it to future projections, using standardized CMIP6 forcing (ECMWF, 2025). For the future projection covering the period 2020–2039, the model is run under the SSP3-7.0 scenario. SSP stands for Shared Socioeconomic Pathways, which are narratives developed to describe possible developments in society, demographics, and economics over the 21st century, considering greenhouse gas emissions and climate change. SSP3 represents a "Regional Rivalry" pathway, characterized by high population growth, limited technological development, and a focus on national security and self-reliance over international cooperation. Each SSP is coupled with an RCP (Representative Concentration Pathway), which describes a possible trajectory of radiative forcing, the difference between incoming solar radiation and outgoing infrared radiation caused by greenhouse gases. In this scenario, the radiative forcing is set at 7 W/m^2 by the year 2100 (Riahi et al., 2017). The projections are initialized in 2020 using reanalysis data, followed by a five-year ocean spin-up. This adjustment phase allows the ocean model to equilibrate and reach a stable state before the projections start (ECMWF, 2025).

Table 2.3: Description of ICON variables used in the analysis

Full Name	**Units**	**Variable Name**	**Detailed Definition**
Total precipitation	$\mathrm{kg\,m^{-2}\,(s^{-1})}$	`tprate`	This parameter is the accumulated liquid and frozen water—comprising rain and snow—that falls on the Earth's surface.
Maximum temperature at 2 m	K	`2t`	This parameter is the highest daily air temperature at 2 m above the surface of land, sea or inland waters.
Minimum temperature at 2 m	K	`2t`	This parameter is the lowest daily air temperature at 2 m above the surface of land, sea or inland waters.

2.5 Data processing

Starting from the data downloaded from the three different datasets, the region of interest is selected by applying spatial (latitude and longitude) and temporal constraints. For ERA5 and BARRA, the historical period considered is 1990–2019. Historical data from ICON is also included for this period. For the future period in the ICON simulation, the selected years are 2020–2039. The selected area lies between 3°S and 25°S latitude, and between 153°E and 195°E longitude (using a 0° to 360° longitude system). This selection was made to allow the analysis of different islands that may show varying responses to climate change, without including the entire PICTs region, which would be too heterogeneous to analyze as a whole. The selected area also makes it possible to account for the local effects of the ITCZ and SPCZ, as well as to analyze their evolution.

For ERA5 and ICON, the data are downloaded at a daily frequency, while for the BARRA dataset,

data are available at a 6-hourly resolution. The BARRA data are converted to a daily frequency: for temperature, daily means of maximum and minimum values are computed by averaging the records from each day; for precipitation, total daily amounts are obtained by summing all available values within the same day.

The data variables are converted from the units of measurement shown in Tables 2.1, 2.2, and 2.3. For daily minimum and maximum temperatures, the conversion from Kelvin to Celsius is performed:

$$T_{^\circ\mathrm{C}} = T_{\mathrm{K}} - 273.15$$

Regarding precipitation, a conversion from meters per hour (m/h) is necessary for the ERA5 data:

$$P\,[\mathrm{kg\,m^{-2}\,day^{-1}}] = P\,[\mathrm{m\,h^{-1}}] \times \frac{1000\ \mathrm{kg}}{1\ \mathrm{m^3}} \times 1\ \mathrm{m^2} \times 24\ \frac{\mathrm{h}}{\mathrm{day}}$$

For ICON, the data is in millimeters per second (mm/s) and were also converted accordingly.

$$P\,[\mathrm{kg\,m^{-2}\,day^{-1}}] = P\,[\mathrm{mm\,s^{-1}}] \times \frac{1\ \mathrm{kg}}{1\ \mathrm{mm\,m^{-2}}} \times 86400\ \frac{\mathrm{s}}{\mathrm{day}}$$

2.5.1 Regridding and bias calculation

To calculate the bias of the ICON model, BARRA and ICON data are compared by computing the means of daily minimum and maximum temperatures, as well as precipitation, over the period 1990–2019. This approach provides a better understanding of how well the ICON model simulates the climatology of the study area. The methods used for daily temperatures and precipitation differ. For daily temperatures, the bias is calculated simply as the difference between the climatologies derived from BARRA and ICON, indicating how far the model deviates from the reanalysis. For precipitation, the bias cannot be expressed as a negative value, so the percentage bias is calculated instead, representing the relative difference from the BARRA precipitation. The following formulas are used for bias calculation (Chen, Brissette, and Lucas-Picher, 2015):

$$B_p\ [\%] = \frac{\overline{P}_{\mathrm{ICON}}\ [\mathrm{mm/day}] - \overline{P}_{\mathrm{BARRA}}\ [\mathrm{mm/day}]}{\overline{P}_{\mathrm{BARRA}}\ [\mathrm{mm/day}]} * 100 \tag{2.1}$$

$$B_t\ [^\circ\mathrm{C}] = \overline{T}_{\mathrm{ICON}}\ [^\circ\mathrm{C}] - \overline{T}_{\mathrm{BARRA}}\ [^\circ\mathrm{C}] \tag{2.2}$$

where all variables $\overline{P}_{\text{ICON}}$, $\overline{P}_{\text{BARRA}}$, $\overline{T}_{\text{ICON}}$, and $\overline{T}_{\text{BARRA}}$ represent the mean values over the period 1990–2019, while B_p is the precipitation bias and B_t is the bias for minimum and maximum temperatures, applying the formulas for each pixel in the area.

Working with different datasets at varying spatial resolutions means dealing with different grids. This poses a challenge when trying to use the datasets together or perform accurate comparisons. A regridding process was applied to the BARRA dataset to match the resolution of ICON. BARRA was selected for regridding because its resolution is closer to that of ICON, whereas regridding from ERA5 would have resulted in a significant loss of information.

For the regridding, the CDO (Climate Data Operators) command-line tool was used. CDO is a collection of operators designed to simplify the analysis and processing of climate and numerical weather prediction data. It enabled the extraction of the ICON grid and, through first-order conservative remapping Schulzweida, which strictly conserves the integral of transferred quantities such as mass or energy (Jones, 1999), the regridding of the BARRA-R dataset to match it.

2.5.2 Main Libraries

The data has been managed using Xarray, a powerful Python library that enables working with multi-dimensional arrays. It is particularly well-suited for weather and climate data, offering features such as automatic labeling of plots and support for non-standard calendars. Xarray also integrates with Dask, a powerful library for parallel computing that enables processing memory-intensive datasets (Hoyer and Hamman, 2017). For the calculation of the indices and the percentiles, the Xclim library was used. It is a powerful tool for computing climate-related indicators and integrates efficiently with xarray and the parallel computing capabilities provided by Dask, enabling fast and efficient processing even with large datasets (Bourgault et al., 2023).

3. Methodology

3.1 Introduction

All data management, as well as the creation of maps and graphs, was performed using Python, with the main contributions of the libraries explained in Subsection 2.5.2. This chapter presents the analyses and statistical methods employed to obtain and interpret the results. First, it provides an explanation of the selected indices and the procedures used for their calculation.

For the purpose of this thesis, the data have been divided into three groups: islands, which includes all grid points located on the land; sea, comprising all remaining oceanic pixels; and a third category referred to as the halo, which consists of sea pixels located adjacent to the islands. This classification was carried out using land-sea masks for ERA5 and ICON. Since the BARRA dataset was regridded onto the ICON grid, the same mask could be applied.

For ERA5, the halo includes the two rows of ocean pixels surrounding the islands, while for ICON and BARRA, five rows were used due to the higher spatial resolution of these datasets. This third category—the halo—was defined in order to analyze the potentially distinct climate behavior between the islands and the immediately surrounding ocean. The goal is to understand how climate change may manifest differently even in geographically adjacent regions, and how high-resolution models can help capture these localized differences more effectively.

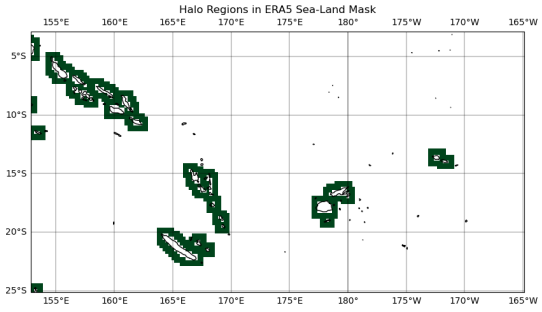

(a) The halo region consists of the two rows of pixels surrounding the land as identified by the sea–land mask in ERA5.

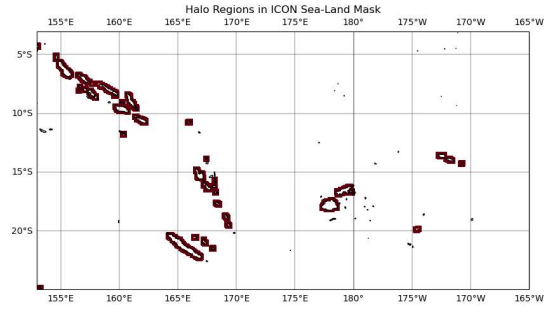

(b) The halo region consists of the five rows of pixels surrounding the land as identified by the sea–land mask in ICON.

3.2 ETCCDI indices

The indices selected to assess changes in temperature and precipitation extremes are the ETCCDI (Expert Team on Climate Change Detection and Indices), which are calculated from daily precipitation and temperature data. This decision is based on several workshops held in past years, starting in 1997, which focused on indices and indicators for climate extremes, described in Zhang et al. (2011). The ETCCDI indices are 27 and they are reported in the following table:

Table 3.1: Description of ETCCDI climate indices. Source: Zhang et al. (2011)

Index	**Description**
FD	Annual count of days when daily minimum temperature (TN) < 0°C.
SU	Annual count of days when daily maximum temperature (TX) > 25°C.
ID	Annual count of days when TX < 0°C (icing days).
TR	Annual count of days when TN > 20°C (tropical nights).
GSL	Growing season length: days between first span of $\geq$ 6 days with mean temp > 5°C and first span after July 1st of $\geq$ 6 days with mean temp < 5°C.
TXx	Monthly maximum of daily maximum temperatures.
TNx	Monthly maximum of daily minimum temperatures.
TXn	Monthly minimum of daily maximum temperatures.
TNn	Monthly minimum of daily minimum temperatures.
TN10p	Percentage of days when TN < 10th percentile.
TX10p	Percentage of days when TX < 10th percentile.
TN90p	Percentage of days when TN > 90th percentile.

Continued on next page

Continued from previous page

Index	**Description**
TX90p	Percentage of days when TX > 90th percentile.
WSDI	Warm spell duration index: annual count of days in spells of $\geq$ 6 consecutive days with TX > 90th percentile.
CSDI	Cold spell duration index: annual count of days in spells of $\geq$ 6 consecutive days with TN < 10th percentile.
DTR	Daily temperature range: monthly mean difference between TX and TN.
Rx1day	Monthly maximum 1-day precipitation.
Rx5day	Monthly maximum consecutive 5-day precipitation.
SDII	Simple precipitation intensity index: mean precipitation on wet days ($\geq$ 1 mm).
R10mm	Annual count of days with precipitation $\geq$ 10 mm.
R20mm	Annual count of days with precipitation $\geq$ 20 mm.
Rnnmm	Annual count of days with precipitation $\geq$ user-defined threshold nn mm.
CDD	Maximum length of dry spell (consecutive days with precipitation < 1 mm).
CWD	Maximum length of wet spell (consecutive days with precipitation $\geq$ 1 mm).
R95pTOT	Annual total precipitation on wet days above 95th percentile.
R99pTOT	Annual total precipitation on wet days above 99th percentile.
PRCPTOT	Annual total precipitation on wet days ($\geq$ 1 mm).

For the purpose of this thesis, only a subset of the indices was selected. The initial selection was based on location; for example, the index ID (counting icing days) is completely irrelevant in areas where the maximum temperature is always above zero. Other indices were

excluded due to their lower significance in that area. Instead of the R95pTOT index, the annual number of days with precipitation above the 95th percentile is computed using the function `xclim.indicators.icclim.R95p` from `xclim`. For simplicity, the resulting index will be referred to as R95p. The final 7 indices selected are reported in Table 3.2

Table 3.2: Selected ETCCDI climate indices used in this thesis. Source: Zhang et al. (2011).

Index	**Units / Type**	**Description**
CDD	days	Maximum length of dry spell, defined as the maximum number of consecutive days with daily precipitation < 1 mm.
R95p	days	Annual days where daily precipitation > 95th percentile (based on 1990-2019 period) of wet days (wet days defined as days with precipitation $\geq$ 1 mm).
CWD	days	Maximum length of wet spell, defined as the maximum number of consecutive days with daily precipitation $\geq$ 1 mm.
TX90p	days	Days where daily maximum temperature (TX) exceeds the calendar day 90th percentile (based on the 1990-2019 period).
WSDI	days	Warm spell duration index: annual count of days with at least 6 consecutive days when TX exceeds the 90th percentile threshold (based on the 1990-2019 period).
TN90p	days	Days where daily minimum temperature (TN) exceeds the calendar day 90th percentile (based on the 1990-2019 period).
TR	days	Number of tropical nights: annual count of days when daily minimum temperature (TN) exceeds 20°C.

The CDD and CWD indices are useful for monitoring impacts on agriculture and water availability, especially since the small size of the islands often means they lack a groundwater basin.

These indices are important for assessing drought periods, along with the R95p index, which relates to the increasing frequency of tropical cyclones and flooding. TX90p and WSDI can help forecast heat waves, which are very dangerous for public health. Along with TN90p and TR, these indices affect the livelihood of people as well as local flora and fauna.

3.3 Statistical methods

The statistical methods described in the following sections are applied both to the raw data and to the derived indices, considering the period from 1990 to 2019 for the historical datasets (ERA5, BARRA-R, and ICON historical) and the period from 1990 to 2039 for the entire time span covered by the ICON data.

3.3.1 Trend and Detrend Calculation

At the beginning, two main approaches for trend analysis were considered. The first approach involved calculating trends using a linear relationship (Klein Tank and Können, 2003) with linregress from the python package `scipy.stats`, while the second approach considered the Mann–Kendall test, which is generally more robust as it does not require the data to follow a normal distribution (Fernández-Duque et al., 2024). Since the results from both tests were consistent, linregress was chosen due to the large volume of data and its computational efficiency. The linregress function performs a linear least-squares regression between two sets of measurements, typically time versus a variable. It returns the slope, intercept, correlation coefficient, p-value, and standard error of the slope (Developers, 2025).

The results used are the slope and the p-value: the p-value evaluates whether the slope is significantly different from zero. Linregress calculates it with a Wald test on the slope, assuming that the test statistic follows a t-distribution (Developers, 2025). The null hypothesis is that the slope equals zero (i.e., no trend), and a small p-value indicates a statistically significant trend.

To better understand the climate and its internal variability, a detrending calculation is performed. For this purpose, the annual mean of the daily maximum and minimum temperatures is computed. A linear regression, calculated similarly to the trend, is then removed from the annual values. This allows the standard deviation to be computed, indicating the strength of the internal variability, with higher values corresponding to stronger variability (Merkenschlager et al., 2021).

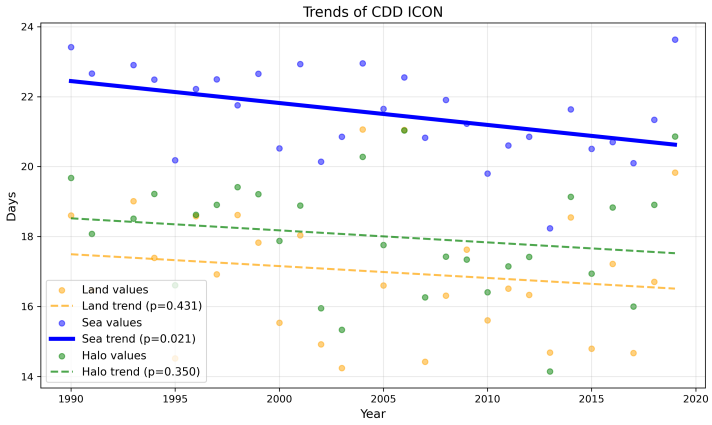

Figure 3.2: Example of a trend in the CDD index calculated with ICON data for the period 1990–2019. A continuous line indicates a statistically significant trend ($p < 0.05$), while a dashed line indicates a non-significant trend.

3.3.2 Probability Density Function

Changes in the Probability Density Function (PDF) from past to present data can provide important insights into how the climate and its extremes are evolving, as shown in Figure 3.3 (Perkins et al., 2007).

In this work, probability density functions (PDFs) are computed for precipitation and maximum and minimum temperature data. Daily values are used, and the PDFs are estimated using the `kdeplot` function from the `Seaborn` library. `Seaborn` provides a high-level interface for creating attractive and informative statistical visualizations (M. L. Waskom, 2021). Specifically, the `kdeplot` function is used to visualize univariate or bivariate distributions through kernel density estimation, a technique that represents the data as a smooth, continuous probability density function in one or more dimensions (M. Waskom, 2024).

Along with the distribution curve, the mean and standard deviation are evaluated. The mean is computed for all variables, whereas a different approach is used to assess variability: for temperature data, the standard deviation is computed; for precipitation, which does not follow a Gaussian distribution, the interquartile range (IQR) is used due to the asymmetry of the distribution (Schwarzwald et al., 2021; Mearns et al., 1995), and is calculated as:

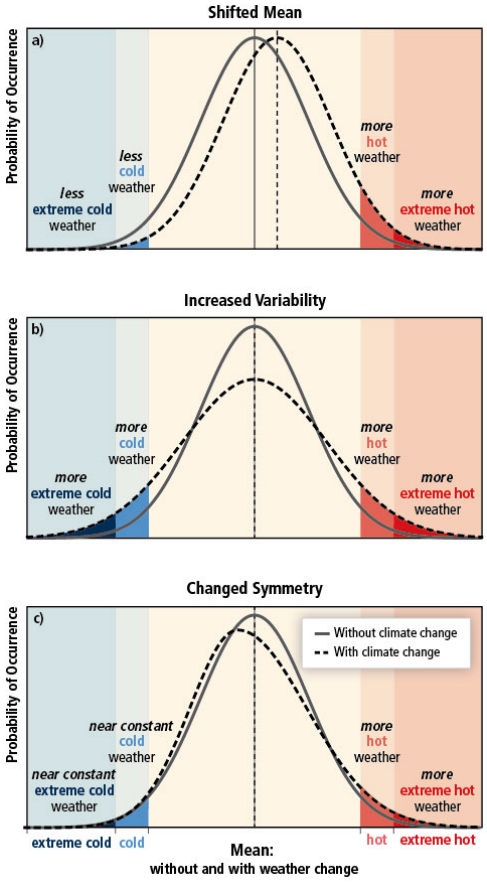

Figure 3.3: The effect of changes in temperature distribution on extremes. Different changes in temperature distributions between present and future climate and their effects on extreme values of the distributions: (a) effects of a simple shift of the entire distribution toward a warmer climate; (b) effects of an increase in temperature variability with no shift in the mean; (c) effects of an altered shape of the distribution, in this example a change in asymmetry toward the hotter part of the distribution. Source: IPCC (2012)

$$\text{IQR} = Q_3 - Q_1 \tag{3.1}$$

with Q_3 and Q_1 representing the 25th percentile and the 75th percentiles, respectively.

3.3.3 Permutation Test

A permutation test is conducted to evaluate the statistical significance of the difference in trends observed between the islands and halo regions (see the introduction of chapter 3). To assess whether the difference between the trends observed in the islands and halo regions is statistically significant, two groups are defined: one consisting of all pixels located on the islands (land), and the other composed of an equal number of randomly selected pixels from the halo region. For each pixel, the linear trend is calculated. An iterative procedure is then performed 1,000 times: in each iteration, two random pixels, drawn from either group, are selected, and the difference in their trends is computed. This process is repeated until a distribution of 1,000 pairwise differences is obtained. Finally, this distribution is compared to the observed difference between the land and halo means, and a p-value for a two-sided test is calculated to assess statistical significance. As described in Holt and Sullivan (2023), the p-value is defined by evaluating how often the differences obtained from the random samples are at least as extreme as the observed difference:

$$\text{two-sided } p\text{-value} = P_{H_0}\left(|T| \geq |T_{obs}|\right) \tag{3.2}$$

If the p-value is below the threshold of 0.05, the difference is considered statistically significant, indicating that the behavior of the land and the adjacent ocean differs under the pressure of climate change.

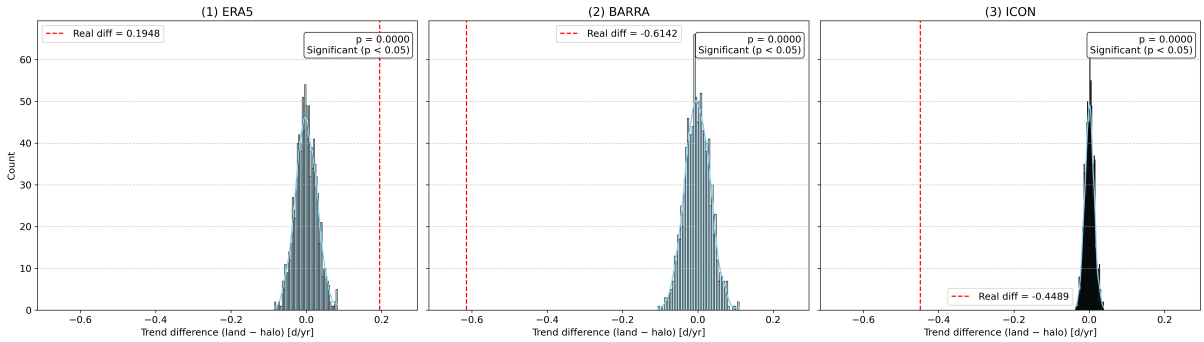

Figure 3.4: Example of permutation test (from left to right) conducted for TN90p index using ERA5, BARRA, and ICON data. The dashed line represents the observed difference (land–halo), while the bars represent the differences obtained through the test.

4. Results

4.1 Introduction

To gain an overview of the changes occurring in the Pacific Ocean, the precipitation trend is calculated using monthly ERA5 data from the period 1940 to 2023.

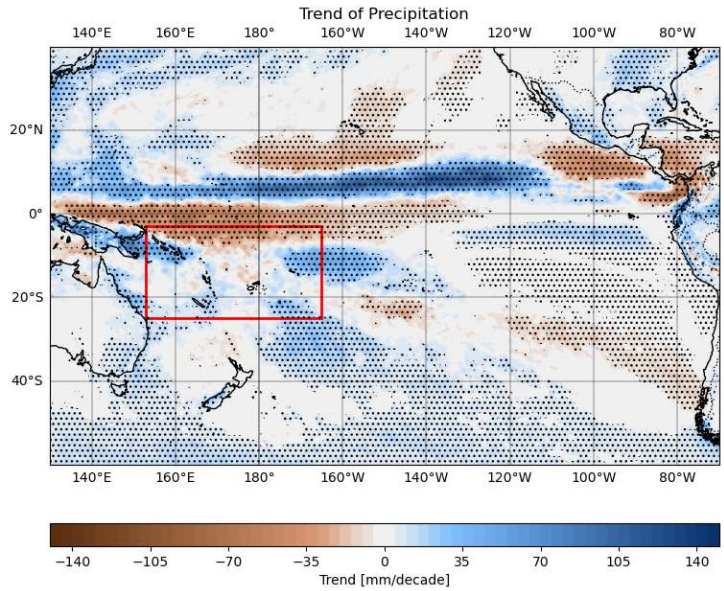

Figure 4.1: Trend in daily precipitation rate over the Pacific Ocean for the period 1940–2023, based on ERA5 data. Black dots indicate statistically significant areas ($p < 0.05$).

From the figure 4.1, and considering Figure 1.4, it is possible to observe that, in the region where the ITCZ is located, a drying phenomenon is occurring in the southeastern part, while a wetting phenomenon is present in the northern part. Meanwhile, in areas where the SPCZ is located, precipitation is increasing in certain regions.

Also the trend for daily maximum and minimum temperature above the Pacific Ocean are computed for the period 1950-2023 using monthly ERA5 data.

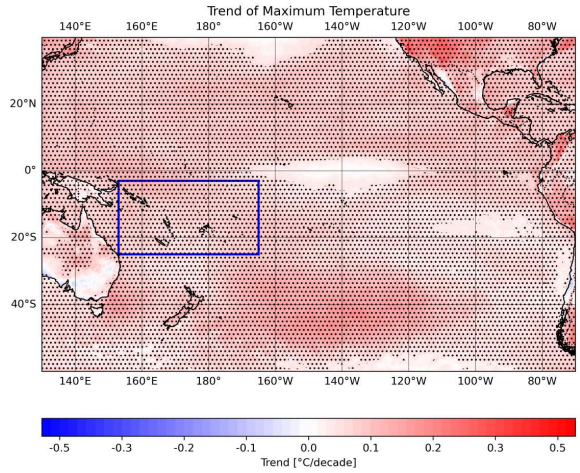

(a) Trend in daily maximum temperature over the Pacific Ocean for the period 1950-2023, based on ERA5 data. Black dots indicate statistically significant areas (p<0.05).

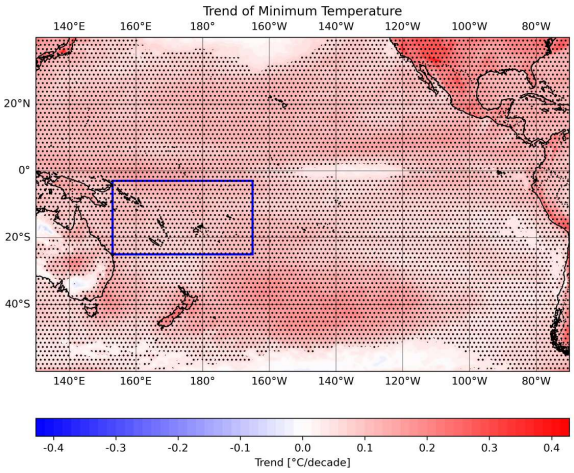

(b) Trend in daily minimum temperature over the Pacific Ocean for the period 1950-2023, based on ERA5 data. Black dots indicate statistically significant areas (p<0.05).

An overall increase in both daily minimum and maximum temperatures is observed across the Pacific region. The trend appears weaker around 20°S latitude, particularly near the coast of South America, likely due to the cold tongue phenomenon. Both daily maximum and minimum temperatures are increasing at a similar rate of approximately 0.1–0.2°C per decade over the area of interest.

In the following sections the focus will be on the selected region of the PICTs area, indicated by the red and blue boxes in the previous figures.

4.2 Comparison between historical data ERA5, BARRA and ICON (1990-2019)

As explained at the beginning of Chapter 2, the three datasets have different spatial resolutions: ERA5 at 25 km, BARRA at 12 km, and ICON at 5 km. The first analysis aims to determine whether this increase in resolution improves the understanding of climate variables and their behavior across the three different groups: islands, halo, and sea.

4.2.1 Precipitation: Climatology and trends

The selected area, as explained in Section 1.1, is crossed by the SPCZ and influenced by the ITCZ in the northeastern part, as shown in figure 2.1.

The precipitation rate in the area reaches 18 mm/day around 10°S latitude, where ICON identifies the location of the SPCZ, and also over the islands. The maps show some pixels with precipitation values far exceeding 18 mm/day, and even surpassing the physically realistic range for that area, likely due to an overestimation of precipitation in the simulation. This point will be discussed further in order to provide a preliminary validation of the ICON model.

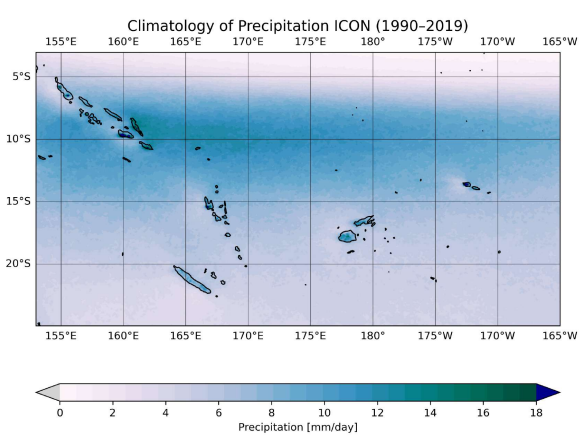

(a) Daily precipitation rate over the area of interest for the period 1990–2019, based on ICON data. Pixels with values above 18 mm/day are highlighted in dark blue.

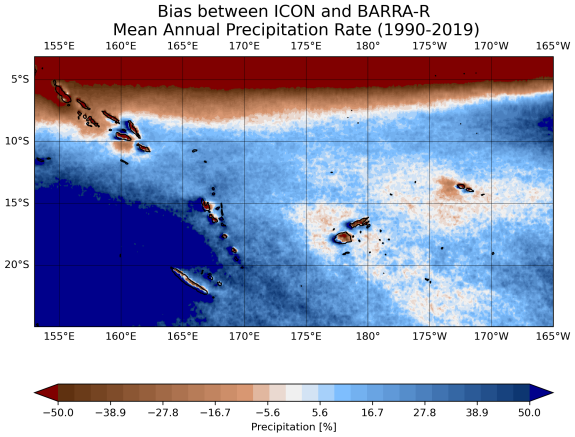

(b) Bias calculated between ICON and BARRA-R daily precipitation over the period 1990 to 2019, using the formula in Equation 2.1. Values exceeding $\pm 50\%$ are colored accordingly in maroon and dark blue

Figure 4.3b shows the difference between ICON and BARRA climatologies. Compared to BARRA, ICON underestimates precipitation in the upper region, where the ITCZ is located, and over the islands. In contrast, precipitation is overestimated in the rest of the ocean. This suggests that the ITCZ is displaced differently in the ICON simulation, as visible in the precipitation climatologies of BARRA (Figure 4.4c) and ERA5 (Figure 4.4a).

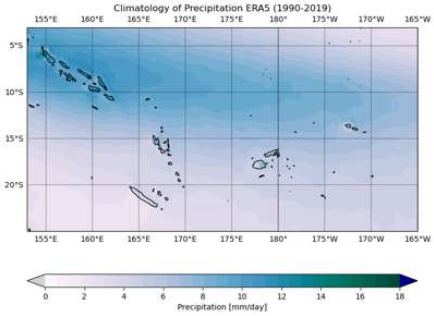

(a) ERA5: Daily precipitation (1990–2019).

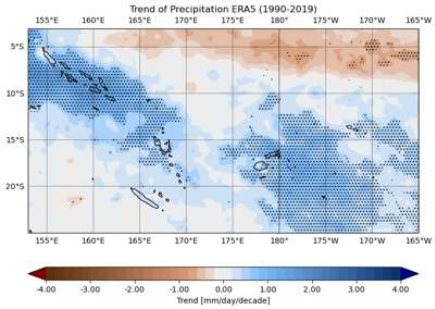

(b) ERA5: Precipitation trend (1990–2019).

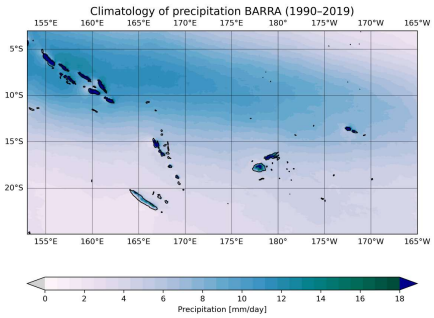

(c) BARRA: Daily precipitation (1990–2019).

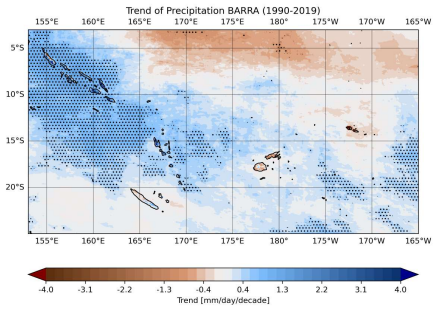

(d) BARRA: Precipitation trend (1990–2019).

Figure 4.4: Comparison of daily precipitation and precipitation trends over the area of interest for the period 1990–2019, based on ERA5 and BARRA data. The subfigures on the left show the climatologies, with maximum daily precipitation values reaching 18 mm/day (highlighted in dark blue). The subfigures on the right show the precipitation trends, with maximum values exceeding ±4 mm/day; black dots indicate areas with statistically significant variation ($p < 0.05$), and values are colored maroon or dark blue accordingly.

The probability density function (PDF) of the precipitation climatology is computed for each of the three datasets for comparison. The PDFs are separated into islands, halo, and sea regions. For each distribution the median is calculated instead of the mean, in order to avoid disturbances generated from outliers.

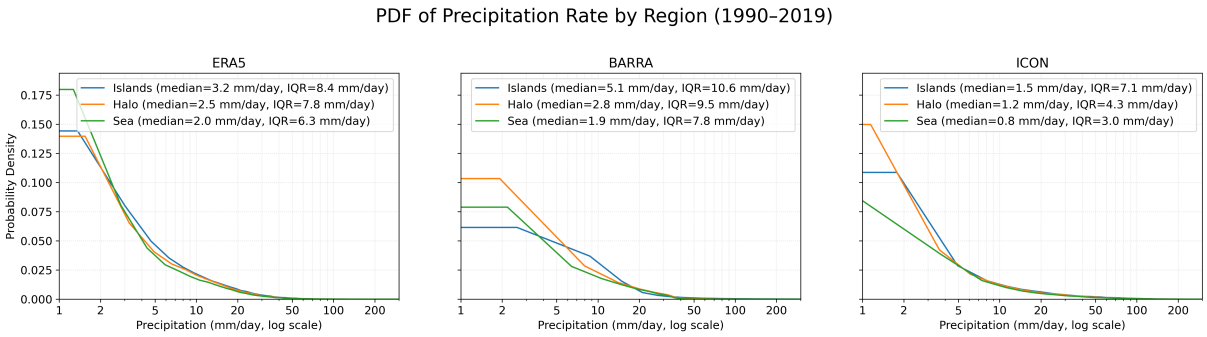

Figure 4.5: Semi-log probability density functions (PDFs) of daily precipitation rate for ERA5, BARRA, and ICON over the period 1990–2019, wit log-xaxis. Islands areas are shown in blue, the halo region in orange, and the sea in green.

Figure 4.5 shows that all three datasets have a higher median and IQR for precipitation over islands, followed by the halo region, with the sea having the lowest values.

In ERA5, the median precipitation values are relatively similar across the three regions, ranging from 2 mm/day over the sea to 3.2 mm/day over the islands. Similarly, ICON shows median values between 0.8 mm/day over the sea and 1.5 mm/day over the islands. BARRA, on the other hand, reports a substantially higher median precipitation over the islands, reaching 5.1 mm/day.

Considering the IQR differences between islands and sea, ERA5 exhibits the smallest gap (2.1 mm/day), followed by BARRA (2.8 mm/day), while ICON displays the largest difference (4.1 mm/day). This indicates that the stronger variability captured by ICON may be related to its higher model resolution, which better distinguishes the variability among the different regions.

The trend is calculated over the period 1990–2019 for ICON, represented in Figure 4.6. A drying trend is observed in the northern part of the map, around 10°S, while in the southernmost part there is an increase in precipitation. However, it is important to note that only a few areas exhibit statistically significant trends. Comparing this map with the trends shown in Figure 2.1, as well as with those reported from ERA5 and BARRA (Figures 4.4b and 4.4d), the drying trend appears to be shifted southward.

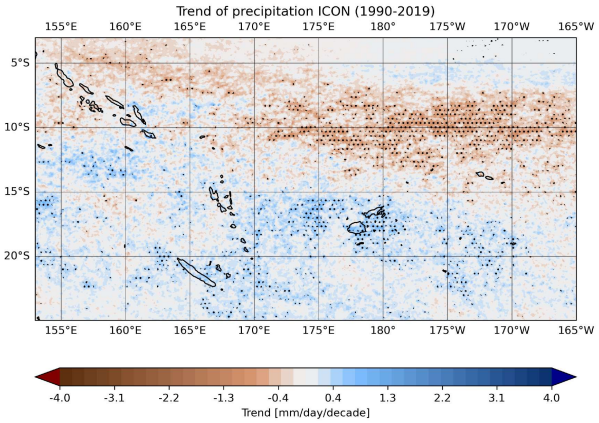

Figure 4.6: Trend of daily precipitation rate over the period 1990–2019, calculated with ICON data. Black dots indicate areas with statistically significant variation ($p < 0.05$). Values exceeding ± 4 mm/day are colored accordingly in maroon and dark blue.

4.2.2 Maximum and Minimum Temperature: Climatology and trend

The PICTs region exhibits very little seasonal variation in daily maximum and minimum temperatures, as previously discussed.

Figures 4.7a and 4.8a show the climatologies of daily maximum and minimum temperatures in ICON. Moving northward from the equator, the mean daily maximum temperature decreases from approximately 29 °C over the ocean near the Solomon Islands to about 22 °C over the islands and at the southern edge of the map. A similar pattern is observed for daily minimum temperature, with values around 17 °C over the islands and up to 27 °C over the northern ocean. The difference between islands and ocean is due to the ocean's higher heat capacity, which allows it to absorb and release heat more slowly, maintaining relatively stable temperatures throughout the year. In contrast, land heats and cools more rapidly, resulting in greater seasonal temperature variations. This effect is particularly noticeable for minimum temperatures, as the ocean exhibits only a small range of variation between day and night (Johnson et al., 2023).

Compared with the BARRA climatology, together with the climatology of ERA5 in Figure A.1, ICON underestimates both daily maximum and, to an even greater extent, minimum temperatures, particularly near the equator (Figure 4.7b and Figure 4.8b). In some island locations, especially in the north, the bias reaches up to 7 °C. Over the ocean, the largest bias is around 4 °C.

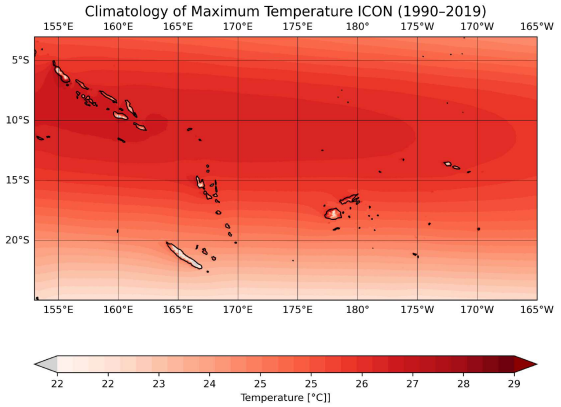

(a) Daily Maximum temperature over the area of interest for the period 1990–2019, based on ICON data. Pixels above 29°C are dark red, below 22°C are light grey.

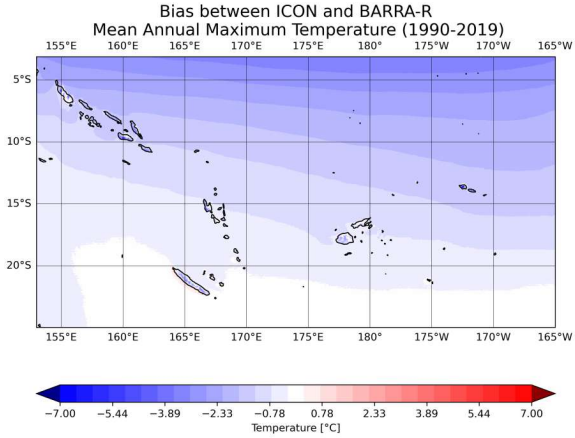

(b) Bias between ICON and BARRA over 1990–2019, using Equation 2.2. Values outside ±7°C are dark blue and dark red.

Figure 4.7: Climatology of daily maximum temperature from ICON and its bias relative to BARRA.

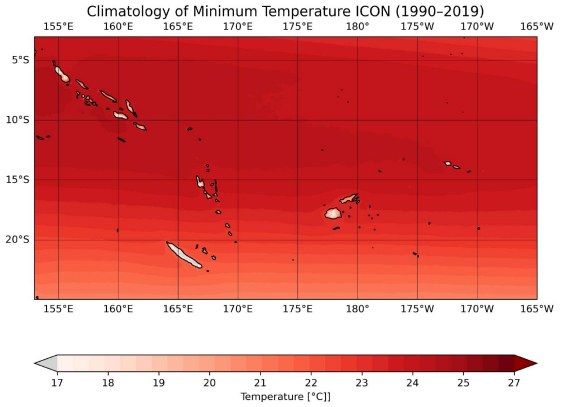

(a) Daily Minimum temperature over the area of interest for the period 1990–2019, based on ICON data. Pixels above 27°C are dark red, below 21°C are light grey.

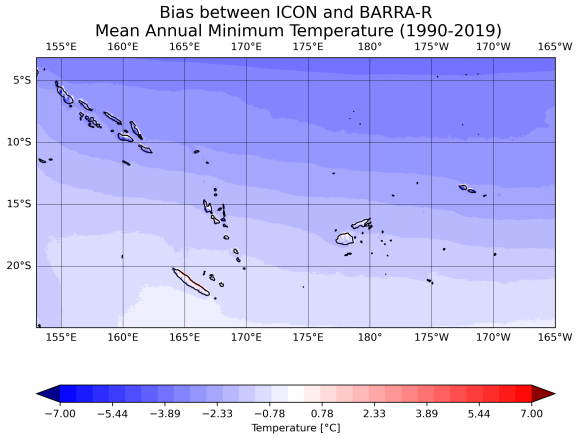

(b) Bias between ICON and BARRA over 1990–2019, using Equation 2.2. Values outside ±7°C are dark blue and dark red.

Figure 4.8: Climatology of daily minimum temperature from ICON and its bias relative to BARRA.

From the PDFs of the three datasets (Figure 4.9), the impact of higher resolution becomes more apparent. In ERA5, the three groups follow almost the same distribution, with the standard deviation of the sea group being higher than that over the islands. However, in BARRA and especially in ICON, the distribution of islands temperature values clearly diverges from the others. A similar pattern is observed for minimum temperature: in ERA5, differences are already noticeable, but they become much more pronounced as the resolution increases. In particular, the distributions indicate lower temperature values (for both maximum and minimum) and greater variability, consistent with the patterns shown in the climatology maps (Figures 4.7a and 4.8a).

The trend calculation for both variables indicates an increase in temperature, in accordance with global warming. The areas with a statistically significant trend are located in the southern part of the map, reaching up to 0.50°C per decade. The results indicate that ICON does not detect a significant increase in temperature near the equator. In ERA5 and BARRA (Figure 4.11), particularly for the daily maximum temperature trend, the north-eastern part of the maps does not exhibit statistical significance, although surrounding areas show a significant trend.

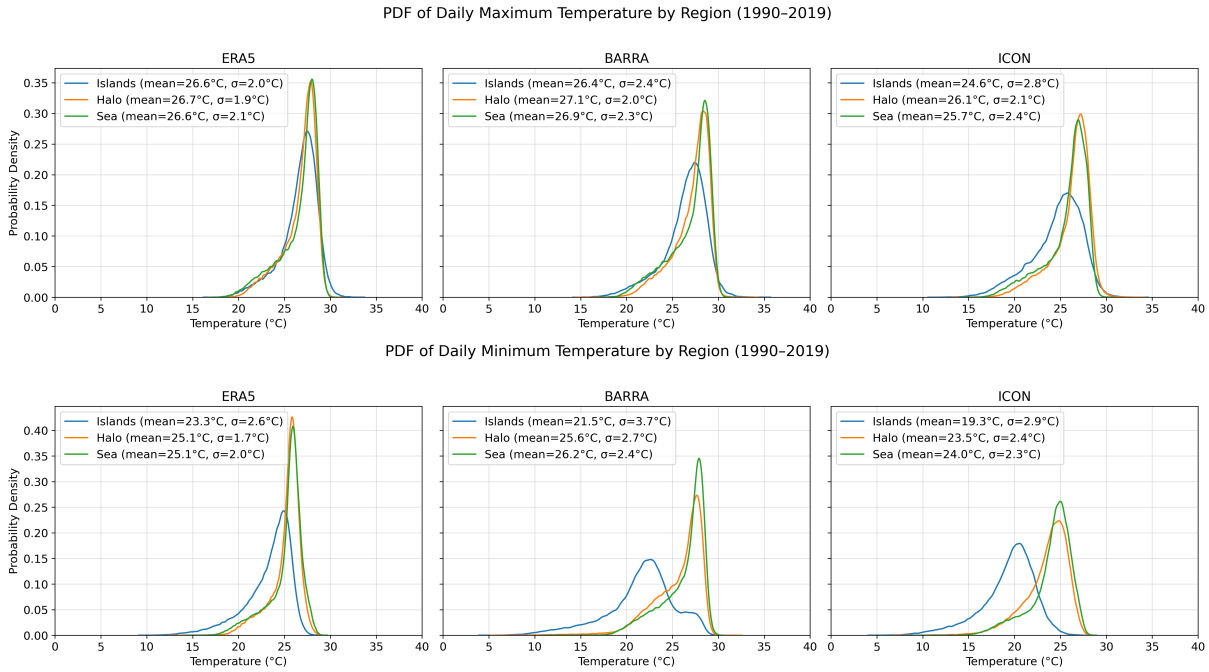

Figure 4.9: Probability density functions (PDFs) for ERA5, BARRA, and ICON over the period 1990–2019 of daily maximum and minimum temperature. Islands areas are shown in blue, the halo region in orange, and the sea in green.

To explain the differences in statistically significant areas between the three datasets and the absence of significance in the north-eastern part, the standard deviation of daily maximum and minimum temperatures was computed. The results show that ICON simulates greater internal variability than ERA5 in the equatorial zone, which explains the lack of statistical significance. When compared with BARRA, the difference is smaller, but ICON still exhibits a larger standard deviation near the equator (see Figures A.2 and A.3). This higher variability in that region may be related to the cold tongue phenomenon, which is influenced by El Niño and La Niña events. In particular, during La Niña events, cold ocean currents flow from the coast of South America toward Australia, and the temperature range becomes wider than during El Niño. El Niño and La Niña alternate every few years, which could explain the weak signal detected in that region (Cai, 2003). This can also explain the differences between these maps and the climatology of the Pacific Ocean, since the ocean trends are calculated over a longer period (1950–2023), which smooths the ENSO-related seasonality compared to the 30-year evaluation period.

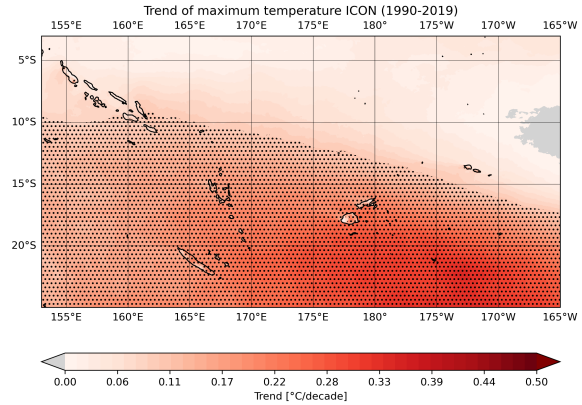

(a) Trend of maximum temperature along the period (1990-2019).

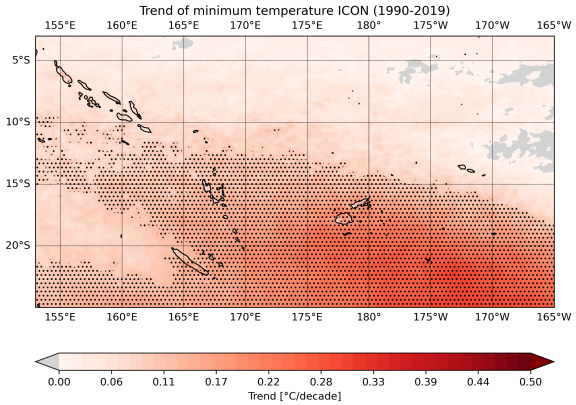

(b) Trend of minimum temperature along the period (1990-2019).

Figure 4.10: Trends of maximum (left) and minimum (right) temperatures during 1990–2019 based on ICON data. Black dots indicate areas with statistically significant variation ($p < 0.05$). Pixels above 0.5 °C/decade are dark red, pixels with negative trend are light grey.

4.2.3 ETCCDI indices

To better understand the possible variation and evolution of extreme events in the area, and how the islands may be affected differently from the surrounding ocean, with consequent social and economic impacts, seven ETCCDI indices are analyzed for the period 1990–2019 using the three datasets.

The indices are computed at yearly frequency. The trend for each index is then evaluated by performing a linear regression on the yearly values, and the resulting trends are divided into three classes: islands, halo, and sea. These graphs show the statistically significant trend of each index, computed through linear regression, with the results reported in Appendix B. If the islands and halo trends are significant, the differences between land and halo are assessed using a permutation test (described in subsection 2.4.1). A p-value below 0.05 indicates a significant difference, meaning that land and the surrounding ocean respond differently to the specific index.

The trends in the indices, shown in Figure 4.12, are sensitive to whether they are computed using the halo, sea, or islands values. Starting from the left, there are the first three indices related

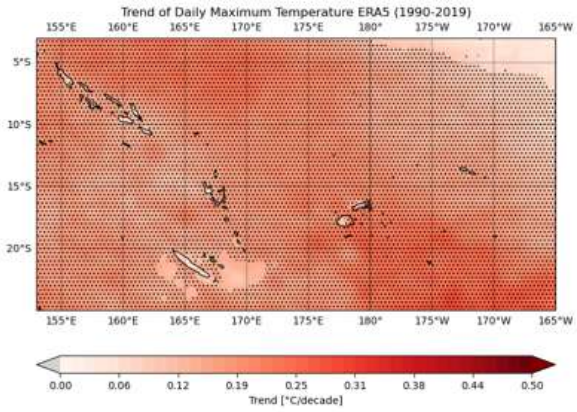

(a) ERA5: Daily Maximum Temperature trend

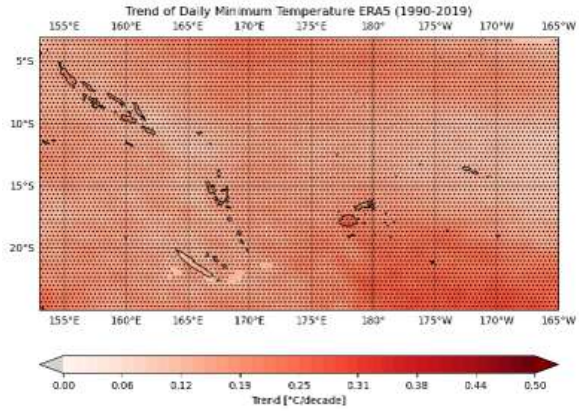

(b) ERA5: Daily Minimum Temperature trend

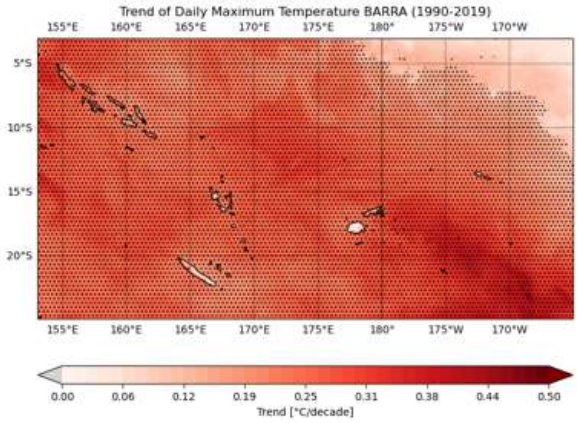

(c) BARRA: Daily Maximum Temperature trend

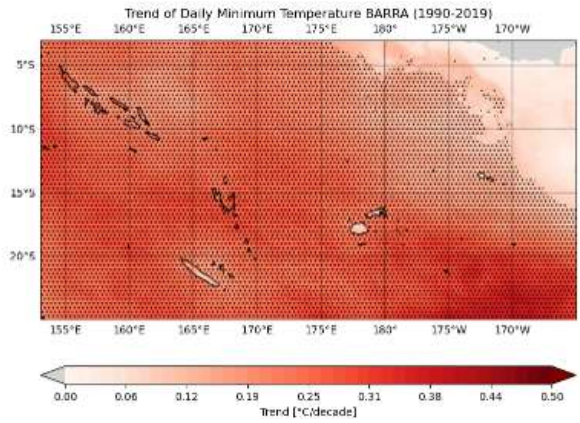

(d) BARRA: Daily Minimum Temperature trend

Figure 4.11: Temperature trends from ERA5 (left) and BARRA (right) for daily maximum (top) and minimum (bottom) temperatures during 1990–2019, over the ICON domain. Black dots indicate areas with statistically significant changes ($p < 0.05$). Pixels with positive trends greater than 0.5 °C/decade are shown in dark red, while negative trends are shown in light grey.

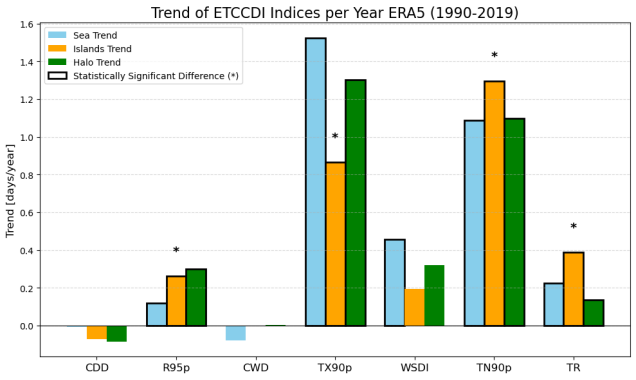

(a) ERA5

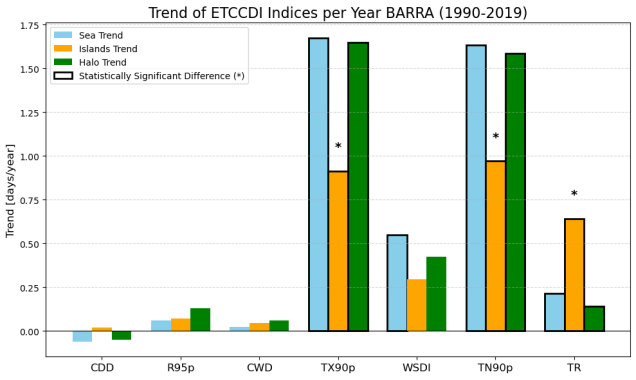

(b) BARRA

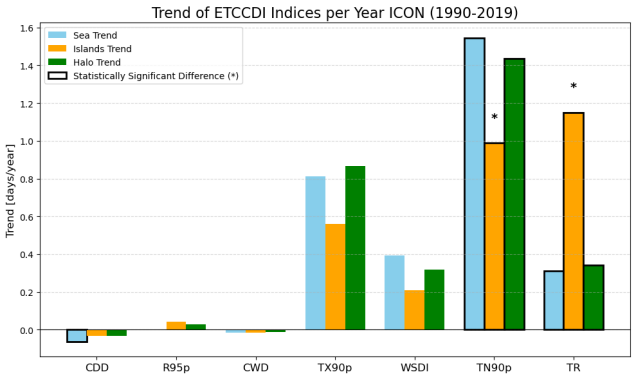

(c) ICON

Figure 4.12: Trends of CDD, R95p, CWD, TX90p, WSDI, TN90p, and TR for the period 1990–2019, based on (from top to bottom) ERA5, BARRA, and ICON. Columns are colored blue for sea areas, orange for islands, and green for halos. Columns with a darker border indicate a statistically significant trend ($p < 0.05$), while an asterisk above indicates a statistically significant difference ($p<0.05$) between land and halo trends.

to precipitation. CDD (Consecutive Dry Days) shows a statistically significant trend only over the sea in the ICON dataset, with a decrease of approximately 0.1 days per year; therefore, the difference between the trends observed over the islands and halo is not computed. R95p (days with precipitation above the 95th percentile) shows statistically significant trends in all three groups, with the highest values over the halo, followed by the islands and sea. A statistically significant difference is also observed between land and halo. CWD (Consecutive Wet Days) show no statistically significant trends in any of the three datasets.

The next two indices relate to maximum temperature. TX90p (days with maximum temperature above the 90th percentile) shows a statistically significant trend in ERA5 and BARRA, with higher values over the sea and halo (around 1.5 days/year) and around 1 day/year over the islands. A statistically significant difference is also observed between islands and halo. In ICON, however, the trends are not statistically significant. WSDI (Warm Spell Duration Index) shows a statistically significant trend only over the sea in ERA5 and BARRA, with a value of approximately 0.5 days per year. For this reason, the permutation test is not performed for this index.

The last two indices, related to minimum temperature, are TN90p (days with minimum temperature above the 90th percentile) and TR (tropical nights, i.e., days with minimum temperature above 20°C). For all three datasets and all three groups, both indices show a statistically significant trend. Both indices show a statistically significant difference between the islands and the halo. For TR, this pattern is consistent across all three datasets, with stronger trends over the islands than over the halo: about 0.4 days/year in ERA5, 0.7 days/year in BARRA, and 1.2 days/year in ICON for the islands, compared with about 0.2 days/year in ERA5 and BARRA and about 0.4 days/year in ICON for the halo.

For TN90p, the ERA5 trend shows a stronger signal over the islands than over the halo (1.3 days/year for the islands vs. 1.1 days/year for the halo), whereas in BARRA and ICON (1 day/year for the islands and around 1.4–1.6 days/year for the halo), the signal is stronger over the halo.

This result may be closely related to the higher resolution of the datasets, as all three can capture the statistical significance of the positive trend. However, ERA5 struggles to accurately represent the response of the islands due to its coarser resolution, a point that will be discussed later. It is important to note that this differing response is already evident in the portion of the sea very close to the islands.

4.3 Projected Climate Change: 1990–2019 vs. 1990–2039 (ICON Model)

In this section, the focus is on the future evolution of climate extremes as projected by ICON. The 1990-2019 period is used as climatological benchmark for comparing future changes. As explained in subsection 2.4.1, the ICON simulation from 2020 to 2039 is run under the SSP3-7.0 scenario. Since the precipitation data contains outliers with highly improbable values, which will be discussed, the median is calculated instead of the mean.

4.3.1 Precipitation: PDFs and trend

Figure 4.13 shows the Probability Density Functions (PDFs) of precipitation in the islands, halo, and sea regions. These groups are analyzed for two different periods, 1990–2019 and 2020–2039. For each period, the median and interquartile range are computed to assess how changes in the distribution affect climate extremes (as illustrated in Figure 3.3).

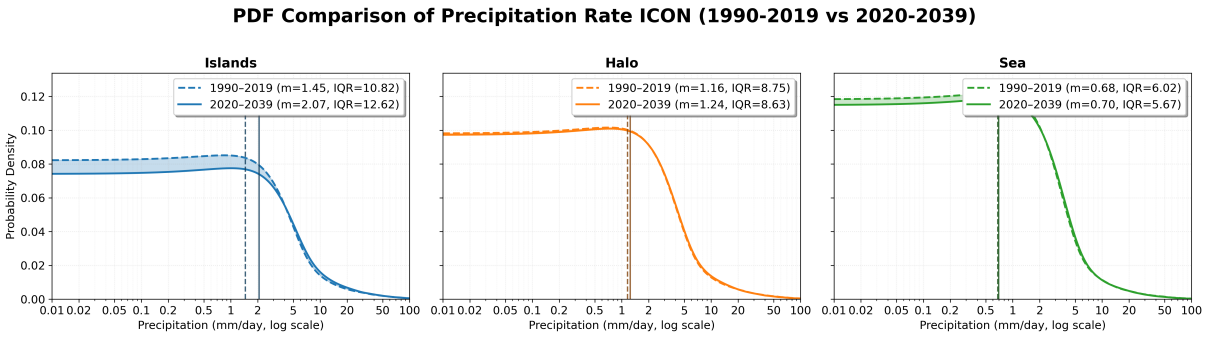

Figure 4.13: Semi-log Probability density functions (PDFs) of daily precipitation rate from ICON data for the periods 1990–2019 (dashed lines) and 2020–2039 (solid lines). Results are shown for islands (blue), halo (orange), and sea (green).

From the three PDFs, it is evident that the islands exhibit higher variability in precipitation rates, both historically and in the future, as indicated by the IQR. This higher variability was also observed in Figure 4.5 from the BARRA and ICON datasets. Halo and sea exhibit lower variability, with the sea showing the lowest values overall. In all three regions, the median precipitation shifts positively, most notably over the islands, where the median exceeds that of

the other two areas. The IQR increases over the islands, while over the halo and the sea it shows a slight decrease from the past to the future.

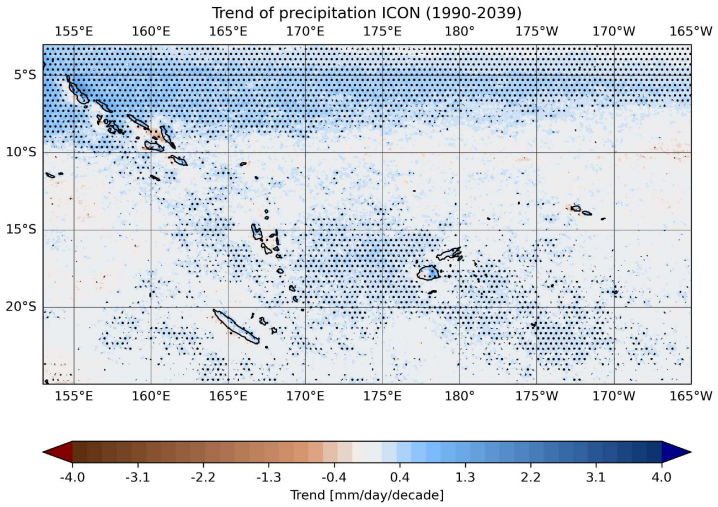

Figure 4.14: Trend in precipitation rate for the period 1990–2039, based on ICON data. Values outside ±4mm/day/decade range are maroon and dark blue. Black dots indicate statistically significant areas ($p < 0.05$).

Figure 4.14 shows the spatial pattern of trends along the period 1990-2039. Compared to Figure 4.6, it reveals a markedly distinct trend in the northern part of the map. For the period 1990–2019, ICON projects a negative trend, whereas for 1990–2039 it becomes positive and statistically significant across the entire northern region. This change is particularly pronounced over the Solomon Islands in the northwest, where precipitation increases by up to 4 mm/day per decade.

4.3.2 Daily Maximum and Minimum Temperature: PDFs and trend

Similar to precipitation, both daily maximum and minimum temperatures exhibit a positive shift in their mean values along with an increase in standard deviation (Figure 4.15 and Figure 4.16).

This change in distribution between the periods 1990–2019 and 2020–2039 is a clear manifestation of climate change, reflecting a rise in both daily minimum and maximum temperatures, as indicated by the mean shift (greater than 1 °C in all cases). Consistent with the climatology, islands exhibit the lowest mean values for both daily maximum and minimum temperatures. In

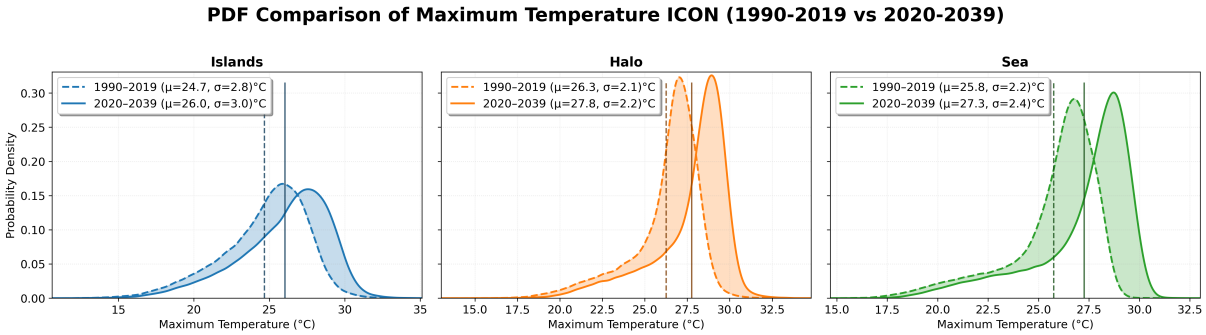

Figure 4.15: Probability density functions (PDFs) of daily maximum temperature from ICON data for the periods 1990–2019 (dashed lines) and 2020–2039 (solid lines). Results are shown for islands (blue), halo (orange), and sea (green).

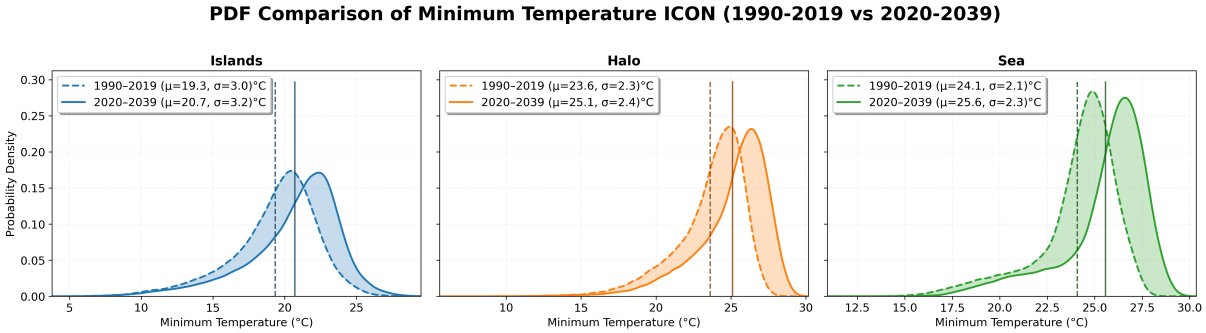

Figure 4.16: Probability density functions (PDFs) of daily minimum temperature from ICON data for the periods 1990–2019 (dashed lines) and 2020–2039 (solid lines). Results are shown for islands (blue), halo (orange), and sea (green).

terms of variability, islands also show a higher standard deviation than halo and sea, reflecting their lower heat capacity, as discussed earlier.

It also points to a greater occurrence of climate extremes, as shown by the increased variability. This is driven by an extension of the upper tail of the probability distribution and a reduction of the lower tail, which together indicate a higher frequency of extreme warm events in daily minimum and maximum temperatures, accompanied by a decline in cold extremes (Robeson, 2002).

Computing the trend for the period 1990-2039, there is a clear increasing temperature signal all over the region (Figure 4.17).

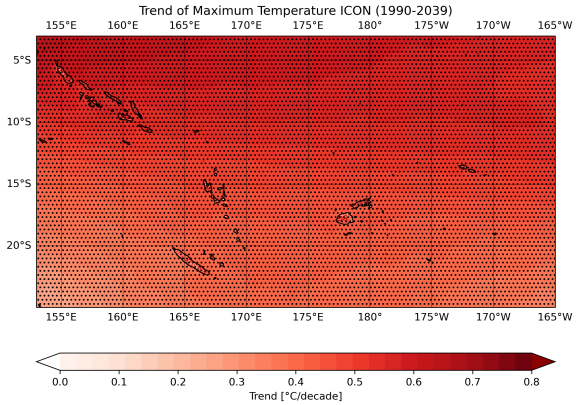

(a) Trend in daily maximum temperature (1990–2039) based on ICON data.

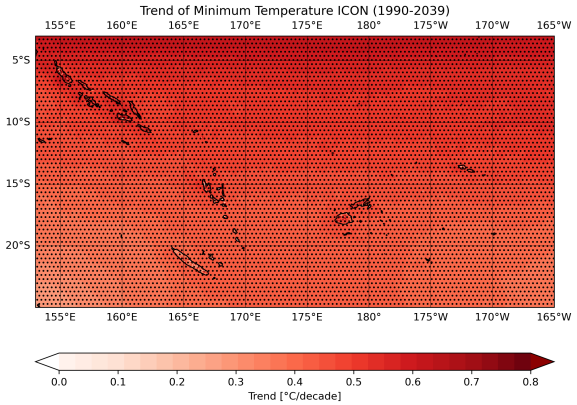

(b) Trend in daily minimum temperature (1990–2039) based on ICON data.

Figure 4.17: Temperature trends from ICON data (1990–2039). Pixels above 0.5°C/decade are shown in dark red, while pixels with negative trends are in light grey. Black dots indicate areas with statistically significant trends ($p < 0.05$).

Compared to the trends over the 1990–2019 period (Figure 4.10), the 1990–2039 projections show that almost the entire area experiences trends in both daily maximum and minimum temperatures reaching up to 0.8 °C per decade, with all points being statistically significant. The trend is strongest near the equator and weakens with increasing distance, in contrast to the 1990–2019 period, when statistically significant trends were predominantly located in the south (Figure 4.17.

4.3.3 ETCCDI indices

The trends of the ETCCDI indices are calculated for the period 1990–2039 (Figure 4.18) and compared with the results shown in Figure 4.12.

For the future projections the indices show a statistically significant trend in every group, along with the differences between islands and halo trends. In particular, for the temperature-related indices (TX90p, WSDI, and TN90p), the trend increases from 1 day to a maximum of 7 days

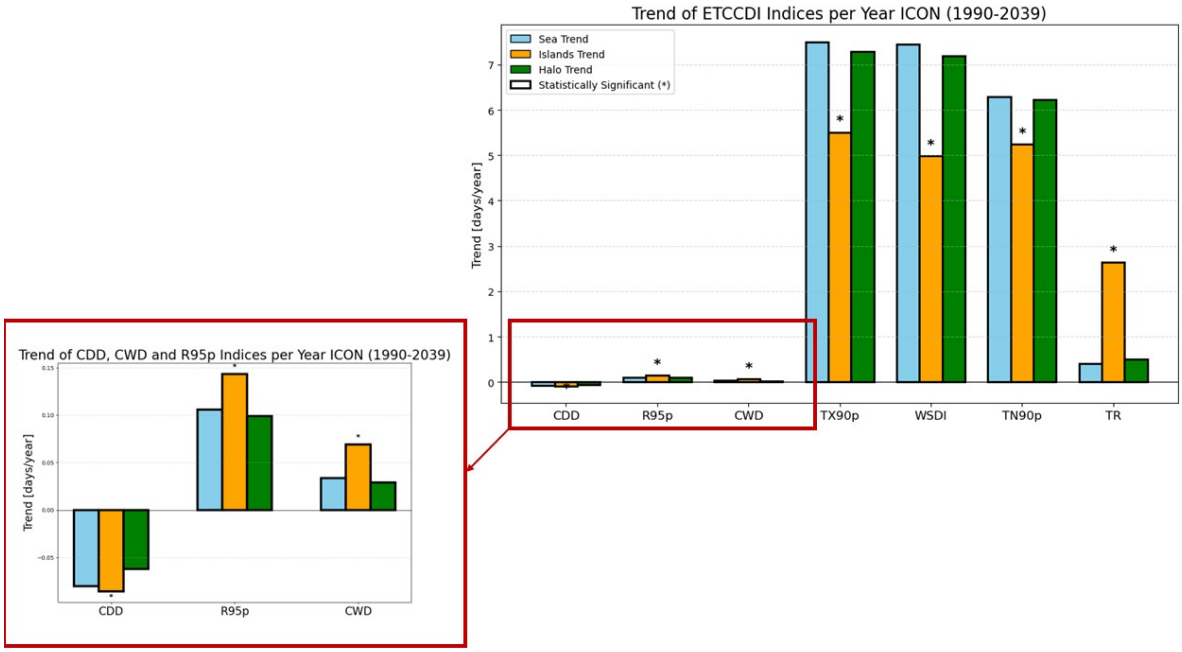

Figure 4.18: Trends of CDD, R95p, CWD, TX90p, WSDI, TN90p, and TR for the period 1990–2039, based on ICON (from left to right). Columns are colored blue for sea areas, orange for islands, and green for halos. Columns with a darker border indicate statistically significant trends, while an asterisk above indicates a statistically significant difference between land and halo trends.

per year for the halo, and 5–6 days per year for the islands. The TR index shows a trend of 0.5 days per year for the halo and 2.5 days per year for the islands. Precipitation-related indices show trends magnitude lower than 1 day per year. Compared to the historical period, the CDD trend shifts from a positive value (with no statistically significant difference between land and halo) to a negative value in the 1990–2039 period, consistent with the trend shown in Figure 4.3a. Wherever ICON showed statistical significance during 1990–2019 (Figure 4.12c), the indices remain significant also in the future period, with consistent trends but stronger increases.

4.3.4 Evolution of climate extremes in three main PITCs cities

In this section is shown the climate evolution over three main cities from three different island groups, as projected by ICON: in the northern part of the region, Honiara in the Solomon Islands;

from the central area, Suva in the Fiji Islands; and in the south, Noumea in New Caledonia.

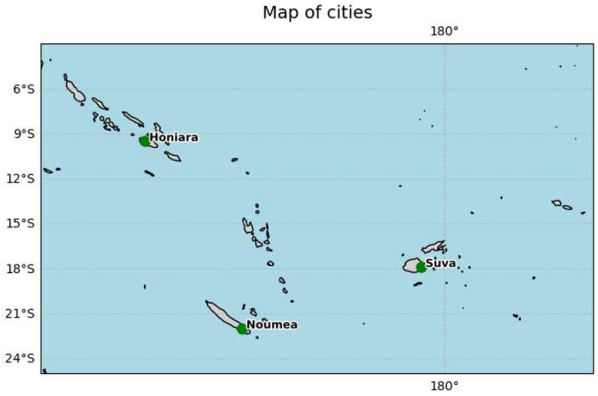

Figure 4.19: Maps of the small Pacific islands and their main cities considered.

For each city location, a corresponding point is also selected in the surrounding sea near the island. This allows the time series of the different variables to be evaluated for both types of areas, highlighting any differences in their behavior under changing climate conditions. From the selected points, a surrounding area of 5 pixels was also included in order to smooth the results and better capture the behavior of that zone. The surrounding pixels were considered only if they belonged to the appropriate group. The selected points are shown in the following maps, together with the land and halo ICON masks (Figure 4.20).

In the following results, the time series of precipitation, temperatures, and ETCCDI indices are presented for both halo and land points. A linear regression is performed for each series, and the corresponding p-value is evaluated. Trends that are statistically significant are shown with colored lines, while non-significant trends are displayed in grey.

Noumea

Figure 4.21 presents the time-series of the variables analyzed for Nouméa, located on New Caledonia in the southern part of the study area.

The precipitation indices do not display statistically significant trends, as was expected from Figure 4.6. By contrast, both maximum and minimum temperatures exhibit positive and significant trends. For minimum temperature, mean values over land increase from below 16 °C in 1990 to

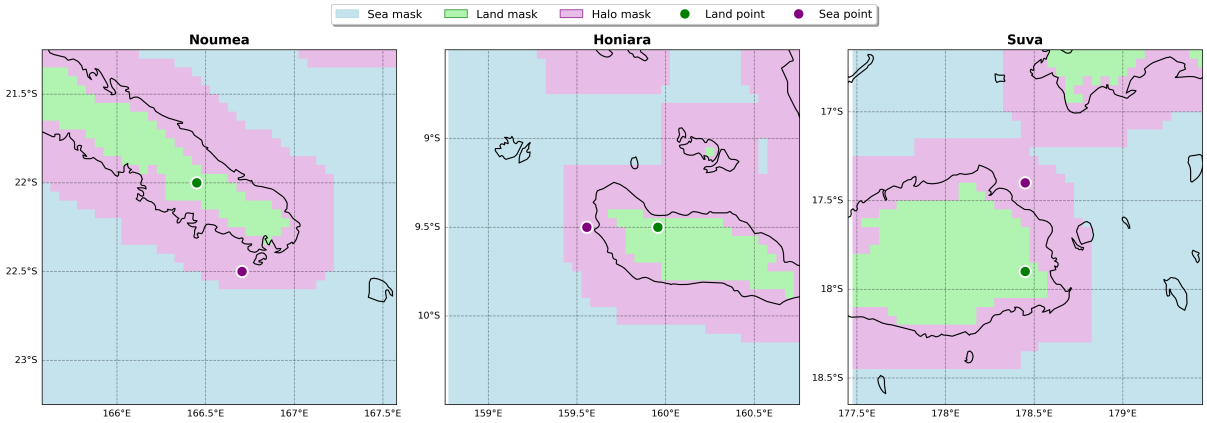

Figure 4.20: Locations of the cities and their corresponding points in the halo are shown. The land mask is displayed in green, while the halo mask is displayed in purple.

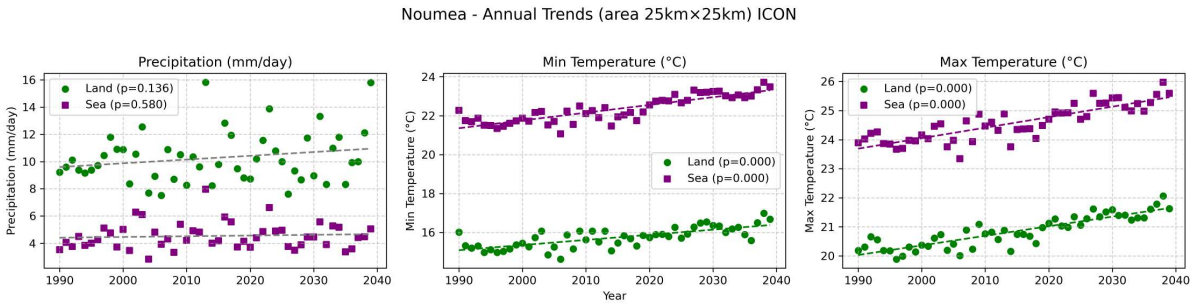

Figure 4.21: Time series of daily precipitation rate, minimum temperature, and maximum temperature from ICON data for the period 1990–2039 in Noumea. Statistically significant trends are shown with colored lines, while grey lines indicate non-significant trends.

nearly 17 °C by 2040, while over the sea they rise from about 21 °C in 1990 to approximately 23 °C in 2040. For maximum temperature, land values increase from around 20 °C in 1990 to almost 22 °C in 2040, whereas sea values rise from about 24 °C to nearly 26 °C over the same period.

Figure 4.22 shows the evolution of the ETCCDI indices in Noumea. The CWD index shows no statistically significant trends. CDD shows negative trends over the sea, indicating that dry

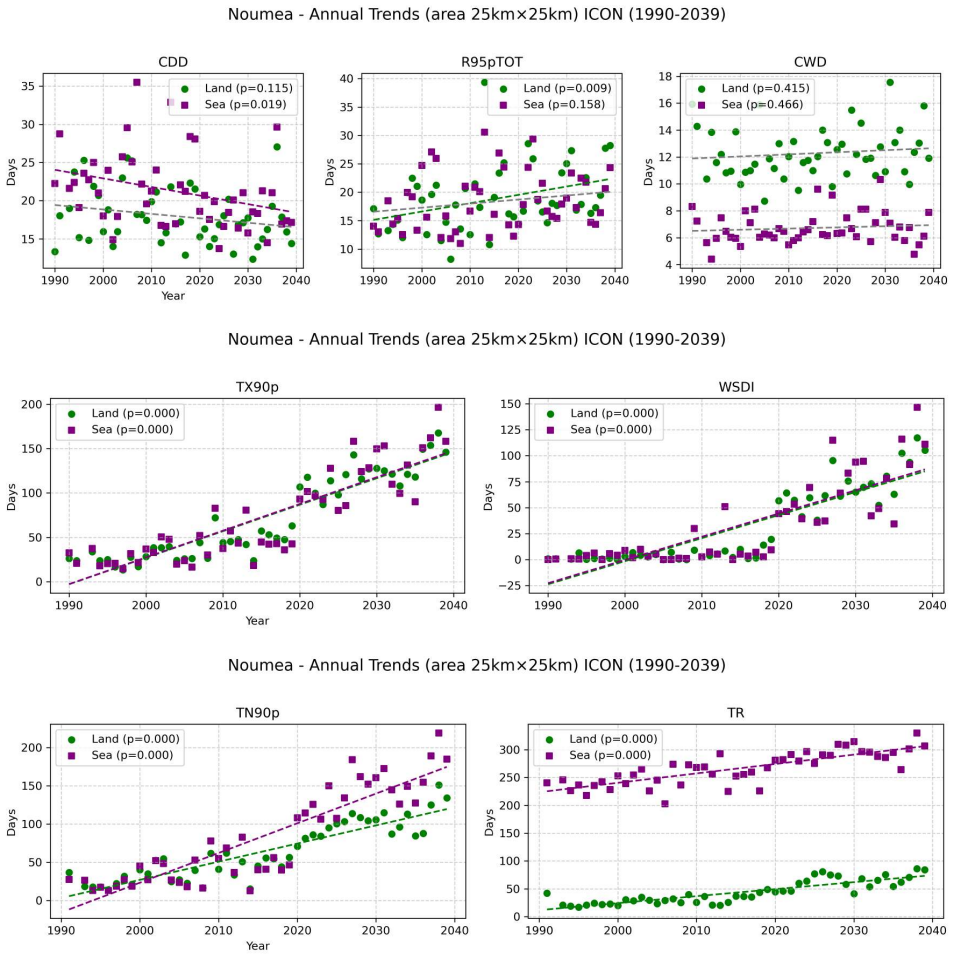

Figure 4.22: Time series of the ETCCDI indices for the land and halo areas of Noumea over the period 1990–2039 from ICON data.

periods have become shorter over time (decreasing from about 25 to 20 days per year). R95p shows a positive trend over land, increasing from about 15 to nearly 25 days per year. TX90p and WSDI both show significant increasing trends, with land and sea exhibiting very similar behavior. In this case, the difference between the ICON historical data and the ICON simulation is particularly pronounced for the WSDI index. For the minimum temperature–related indices, the trends are increasing and statistically significant. TN90p shows a stronger trend over the sea than over land. TR shows a large difference in the number of days between land and sea, although it is smaller than in the other two cities. Over land, the number of tropical nights was close to zero in 1990 and is projected to reach nearly 100 days per year by 2040. Over the sea the value starts from fewer than 250 days and rises to almost a full year by 2040.

Suva

Figure 4.23 presents the time-series of the variables for Suva, located in the Fiji Islands (18°S).

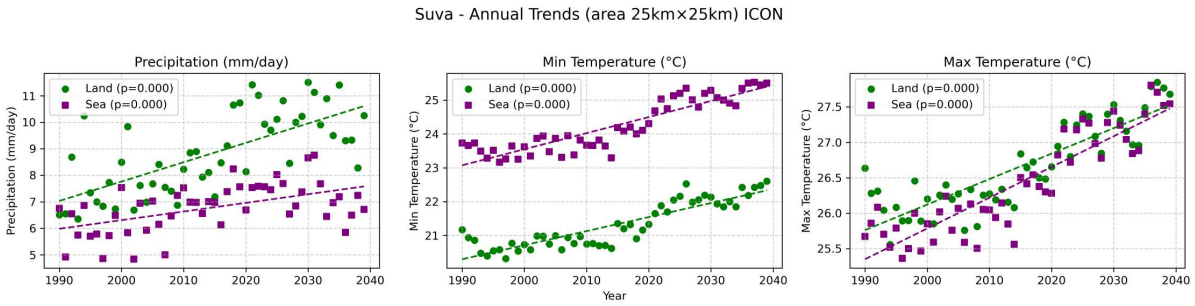

Figure 4.23: Time series of daily precipitation rate, minimum temperature, and maximum temperature from ICON data for the period 1990–2039 in Suva. Statistically significant trends are shown with colored lines, while grey lines indicate non-significant trends.

Precipitation rate shows a significant positive trend over both land and sea, with the difference between the two widening over time as the increase is stronger over land. For minimum temperature, there is a statistically significant difference between land (higher) and sea values, with an increase of more than 2 °C over the 50-year period. Regarding maximum temperatures in Suva, there was an initial difference in 1990, with the sea averaging around 25°C and the land nearly 26°C. Both trends are statistically significant, with the increase over the sea being slightly stronger than over the land, so that by 2040 both reach nearly the same value of 27.5°C.

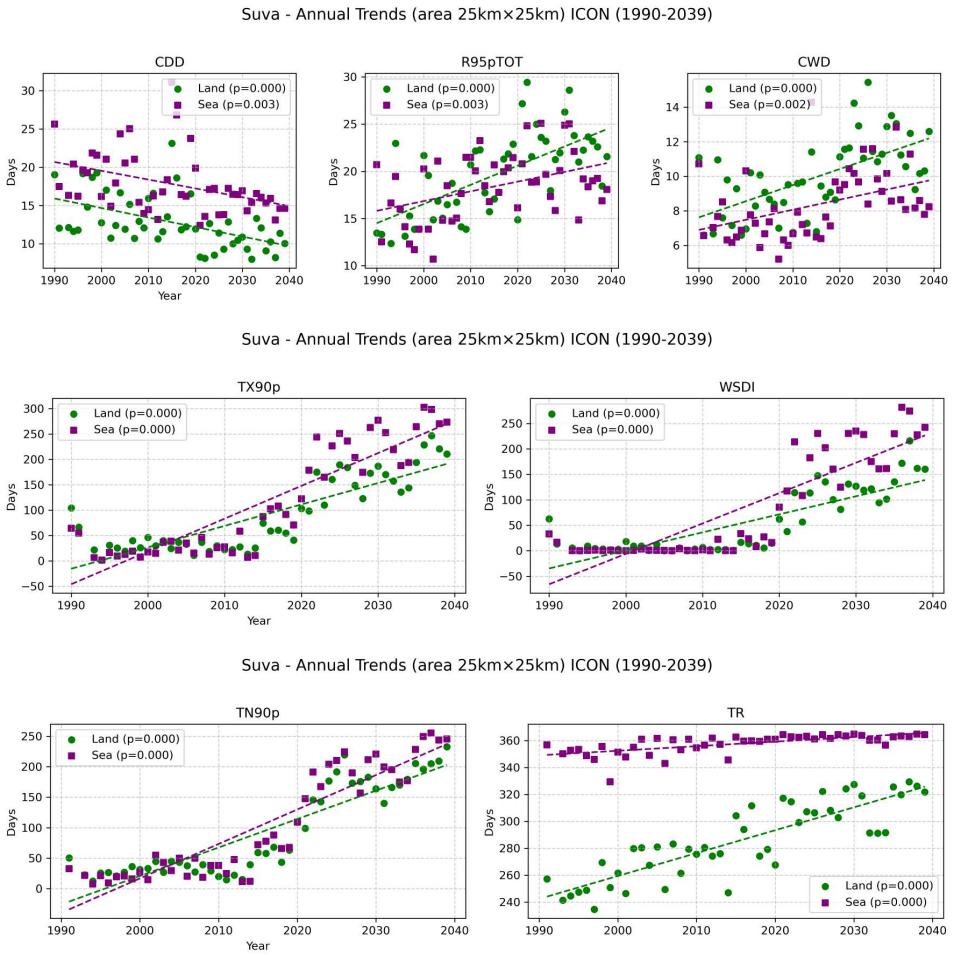

Figure 4.24: Time series of the ETCCDI indices for the land and halo areas of Suva over the period 1990–2039 from ICON data.

All precipitation-related indices show statistically significant trends (Figure 4.24. The CDD index exhibits a decrease and the number of dry days remains higher over the sea than over the land. In contrast, the CWD index is increasing, with a faster rate over land than over sea. The R95p index is also increasing, with a stronger trend over land than over the sea, rising by nearly 10 days over the course of 50 years. For the TX90p and WSDI indices, the trends are statistically significant, with a stronger increase over land than over sea. Compared to Honiara, this difference is even more pronounced. The changes in the ICON simulation are also evident, and some unusually high values are already noticeable in 1990. Looking at the last two indices, the behavior is consistent with what was observed in Honiara. All trends are statistically significant. For TN90p, both land and sea show increasing trends at nearly the same rate, with the trend over the sea slightly stronger than over the land. For TR, the difference is more pronounced: over the sea, the minimum temperature exceeds 20°C almost every day, while over the land, the number of days above 20°C increases from about 240 days per year in 1990 to around 320 days per year by 2040.

Honiara

The time-series of precipitation and maximum and minimum temperatures for Honiara are evaluated in Figure 4.25.

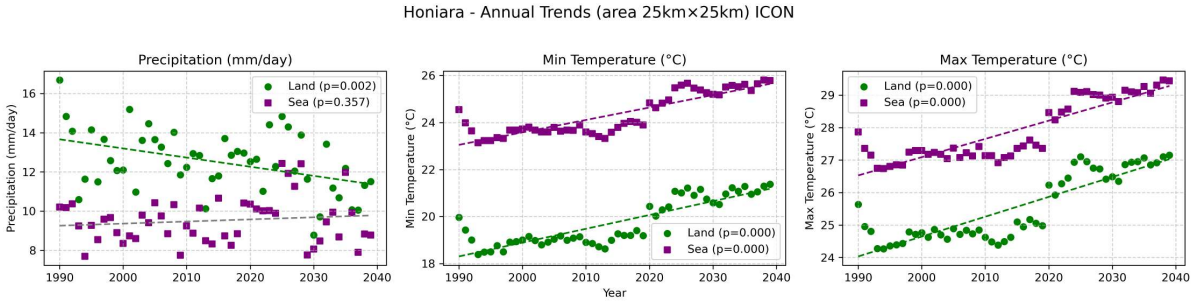

Figure 4.25: Time series of precipitation rate, minimum temperature, and maximum temperature from ICON data for the period 1990–2039 in Honiara. Statistically significant trends are shown with colored lines, while grey lines indicate non-significant trends.

Starting with precipitation trends, no statistically significant changes are observed over the sea, whereas over land the trend is significant and negative. In Honiara, the precipitation rate decreases from about 14 mm/day to around 12 mm/day by 2040. This result is surprising, as the surrounding areas show a statistically significant positive trend, whereas the area around Honiara

exhibits the opposite trend. Both maximum and minimum temperatures show significant positive trends over land and halo. The two curves remain nearly parallel, rising at a similar pace, with maximum temperature showing a steeper increase. In the first years, the values of maximum and minimum temperature are unusually high, and a noticeable shift occurs around 2020, when simulation data begin to be used instead of historical observations.

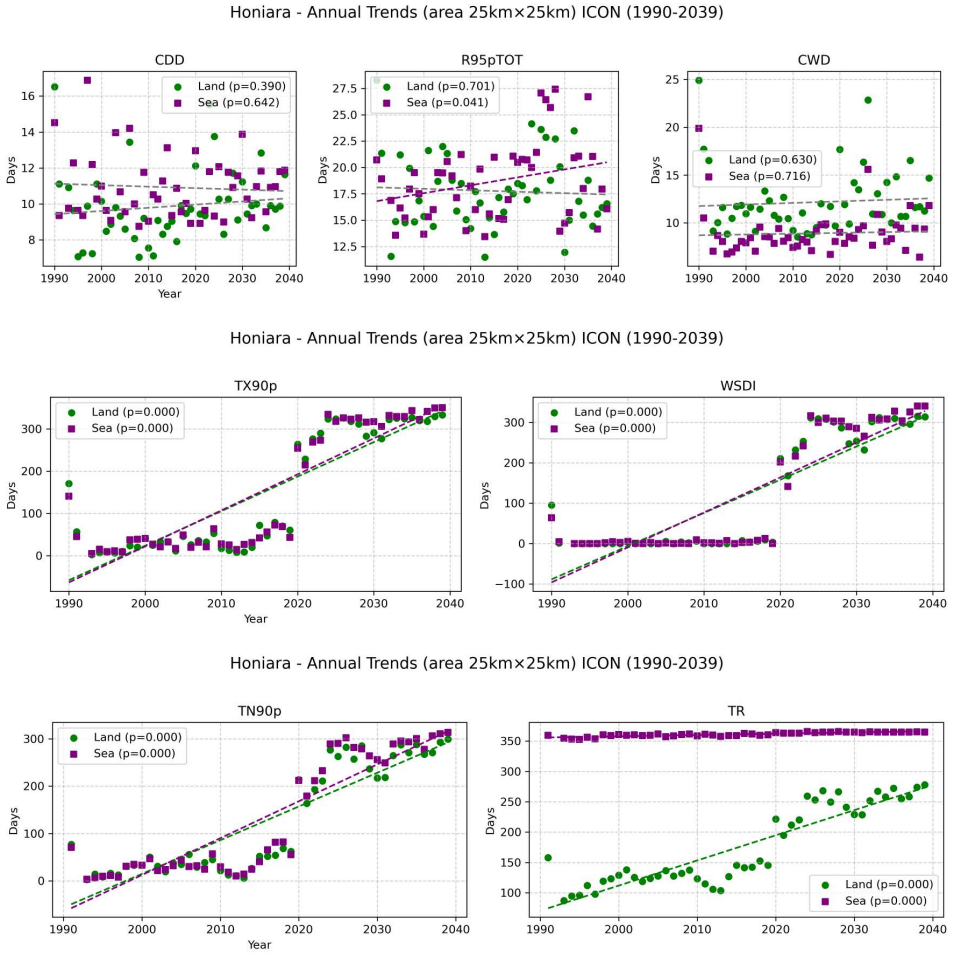

Figure 4.26: Time series of the ETCCDI indices for the land and halo areas of Honiara over the period 1990–2039 from ICON data.

In Figure 4.26, CDD and CWD show no significant trends, whereas R95p exhibits a positive and statistically significant trend only over the halo area. This finding is consistent with the positive precipitation rate trend previously observed in the Honiara region. For the maximum temperature

indices, both land and sea exhibit statistically significant trends in TX90p and WSDI, displaying almost identical behavior, with the two lines nearly overlapping. The time series show very high values during the first two years, followed by a period in which the counts of these indices remain close to zero. After 2020, when the simulation under the SSP3-7.0 scenario begins, the indices increase sharply, reaching values of nearly 300 days per year. For the last two indices, the two trend lines are statistically significant for both the TN90p and TR indices. In the TN90p index, the two lines are nearly coincident; however, toward 2040, the trend over the sea becomes stronger than that over the city. In this case as well, the difference between the two simulations is clearly highlighted. For the TR index, land and sea show distinctly different behaviors. The annual index over the sea is almost saturated, reaching a value very close to 365 days as early as 1990. In contrast, the city began with fewer than 100 tropical nights per year, increasing to nearly 300 days by 2040. A noticeable step is observed around 2020, although it is less pronounced than in the TN90p index.

5. Discussion

5.1 Pacific Ocean Patterns

This thesis aimes to provide a clearer understanding of the extreme climate conditions in the selected PICTs area and their projected evolution in the near future, using a km-scale model for the first time.

Starting with an overview of the Pacific Ocean climate patterns, their observed evolution reported in the literature are consistent with trends obtained from ERA5 data, including a northward shift of the ITCZ (Figure 2.1) and the influence of ENSO on both the position of the SPCZ and temperature increases (Figure 4.2a and Figure 4.2b). These observed trends are linked to the interannual variability of these phenomena, making it crucial to understand their potential behavior in response to increasing CO_2 concentrations and the resulting rise in temperature. This understanding is particularly important for assessing how atmospheric dynamics and the interactions between different phenomena may be affected, given the critical role of the Pacific Ocean in the global climate system (Seager, Henderson, and Cane, 2022). The evolution of large scale patterns in the Pacific Ocean directly impacts the islands scattered across the ocean.

5.2 Effect of spatial resolution

The first part of the results focuses on the effect of a different spatial resolution between ERA5, BARRA and ICON over the historical period (1990-2019).

The analysis of temperature and precipitation PDFs (Figure 4.5, Figure 4.9) highight the difference between a resolution of 25 km (ERA5) to a resolution of 5 km (ICON). The results clearly highlight differences between islands and sea, which become more pronounced in high-resolution ICON compared to ERA5. In contrast, the behavior over halo regions and sea remains very similar.

A characteristic of the data distribution over the islands is its higher variability compared to that over the halo and sea, which is more pronounced in the ICON simulation than in the two reanalysis. This is related to the low heat capacity and thermal inertia of land, where

temperatures change much more rapidly than over the sea, leading to different precipitation patterns and water vapor transport. As a result, there is greater variability in daily maximum and minimum temperatures, influenced by seasonality, and, due to the higher thermal conductivity of land, a greater variability in precipitation rates (Lv, Hao, and Wu, 2023).

The consistent variation observed in the distribution of all three variables highlights the importance of using a high-resolution model. At a coarser resolution such as 25 km in ERA5, the land–sea mask lacks sufficient precision, causing parts of the ocean to be misclassified as land. This issue does not occur when using the land–sea mask in ICON.

Regarding precipitation, the analysis for the period 1990–2019 shows mostly no statistically significant changes, as seen in the trends over time in Figure 4.3a, in the evaluation of the ETCCDI precipitation indices in Figure 4.12c. Moreover, the influence of resolution appears limited, as can be seen in Figure 4.12, which compares all three datasets. This is related to climate drivers whose variability can persist for several years, such as ENSO, MJO, or IPO (Fernández-Duque et al., 2024; Wimhurst and Greene, 2021).

For the ETCCDI indices related to daily maximum temperatures, the ERA5 and BARRA datasets show consistent trends and differences, whereas the ICON dataset does not exhibit statistically significant trends, despite the time series indicating increasing values over the years. The absence of a significant trend may be related to the unusually high values recorded in 1990 by the ICON model, which are likely due to the spin-up phase of the simulation (Figure B.2).

For the indices related to daily minimum temperature, the result for the TR index is consistent across all three datasets. However, for TN90p (days with minimum temperature above the 90th percentile), ERA5 shows a different response compared to BARRA and ICON. In ERA5 the trend is stronger over the islands than over the halo and the sea, whereas in BARRA and ICON the strongest trend appears over the halo/sea. This difference may be a consequence of resolution: ERA5 is less able to distinguish the behavior of the islands from that of the surrounding sea, while ICON and BARRA can capture this distinction more accurately.

This highlights the importance of implementing high-resolution models in the study and prevention of climate change, as they preserve critical information that lower-resolution models may miss.

5.3 Future Projections and Extreme Events

The analysis of the near-future climate projection with ICON reveals a positive shift in the median and an increase in the variability of precipitation, as well as increases in the mean and standard deviation of daily maximum and minimum temperatures (Figures 4.13, 4.15, and 4.16). For precipitation, Figure 4.13 shows a shift in the median, indicating an increase in the daily precipitation rate for 2020–2039 compared to 1990–2019. This pattern is further supported by the trend in Figure 4.14, which, unlike the trend observed for 1990–2019, displays only positive values, pointing to an overall increase in precipitation over the next two decades. Statistically significant signals appear in the trend map near the Equator, in the northern region, and in the central area around the Fiji Islands. These features may be linked to stronger variability and the influence of multiple climate drivers in these regions. Accordingly, recent studies document an increase in drying periods (McGree, Herold, et al., 2019; McGree, Schreider, and Kuleshov, 2016), whereas future projections suggest a rise in wet periods (Iese et al., 2021). This pattern could be connected to the "wet-gets-wetter" mechanism described in the introduction: as temperatures rise, the atmosphere can hold more moisture, intensifying precipitation events, especially in equatorial regions (Dhage and Widlansky, 2022). The increase in variability also leads to a lengthening of the upper tail, with higher values above the 95th percentile, which in turn influences the R95p index. Trends in CDD and CWD further support this picture, showing a decrease in dry periods alongside an increase in wet days. This change, evident when comparing 1990–2019 with 2020–2039, reflects processes that directly shape precipitation climatology. Nonetheless, precipitation-related patterns remain highly complex, and the effects of climate change on them are still uncertain. Extending the analysis period helps to better identify such evolving trends.

From the analysis of the daily maximum and minimum temperature, the shift in the mean is evident in both variables. The direct consequences of this shift is the decreasing in the cold extremes, with the shortening of the bottom tail and the elongation in the upper tail with the increasing in warm extremes. There is also a slightly increase in the variability. The two maps shown in Figure 4.17a and Figure 4.17b display stronger increasing temperature trends, with statistically significant results across the entire area, consistent with the different distributions observed in the PDFs. This elongation in the upper tail indicates an increase in the TX90p and TN90p indices, as more values exceed the 90th percentile. These rising warm extremes are associated with heat waves and with an increase in the Warm Spell Duration Index (WSDI). This is consistent with the results shown in Figure 4.18 for the related maximum and minimum temperature indices. A much stronger increasing trend is observed, rising from about 1 day per

year during 1990–2019 to approximately 6–7 days per year.

From analysis of the three main island cities is possible to better understand how climate change impacts vary depending on location. The precipitation analysis confirms the patterns already highlighted in the trends shown in Figure 4.6.

In Noumea (south), no significant trends are observed in either the precipitation rate or the CDD and CWD indices, with the only exception being R95p over the sea. In Suva (center), located in the Fiji Islands, an increase in the precipitation rate is observed, accompanied by a rise in CWD and R95p, and, as expected, a decrease in CDD. The results indicate that the increase in precipitation and wet days is more pronounced over land than over the sea, consistent with the previous observations. In Honiara (north), ICON projects a decrease in precipitation, although the overall amount remains high due to its geographical location. This localized decline is somewhat unusual, as most of the Solomon Islands show either stable or increasing precipitation, with only a few areas experiencing a decreasing trend.

Considering daily maximum temperature, all three cities show a statistically significant trend. Honiara, located near the Equator, records the highest maximum temperatures and also exhibits the strongest trends in the associated indices. In contrast, Noumea, situated in the southernmost part of the region, shows the lowest maximum temperatures and the weakest trends. Suva presents some unusual climatological features, as the values observed over land and over the surrounding halo are essentially the same. For the daily minimum temperature, the evaluations are very similar to those made for the maximum temperature, with both trends and values decreasing from the Equator toward the south. These results are consistent with the climatologies evaluated both for the wider Pacific region and for the smaller study area considered in this analysis.

Regarding the evolution of the indices, the contrast between land and sea is most pronounced in Suva, where the sea exhibits a stronger trend for TX90p, WSDI, and TN90p. In Honiara and Noumea, by contrast, this land–sea difference is almost negligible. The largest discrepancy is observed for the TR index: over the sea, values have already reached the equivalent of an entire year, whereas over land, they started from low values in each city and are still increasing rapidly.

5.4 Validation of ICON model

The ICON model is part of the Climate DT (*Climate Change Adaptation Digital Twin* 2024) and enables a kilometer-scale analysis of climate extremes (Doblas-Reyes et al., 2025). This study

has made possible to identify some of the strengths and weaknesses of the model. From the climatology of daily precipitation and of daily maximum and minimum temperatures, together with the trend analysis, it is evident that ICON underestimates both maximum and minimum temperatures, while the precipitation distribution differs from that of BARRA and ERA5, highlighting also some points that register very high unusual precipitation rate. In Figure 5.1, some points show values around 30 mm/day, and one point even exceeds 65 mm/day. These values are unrealistic, as data from The World Bank for the period 1990–2019 report an annual precipitation of about 6000 mm, corresponding to an average daily rate of roughly 16 mm/day, which is consistent with the rest of the values shown on the map.

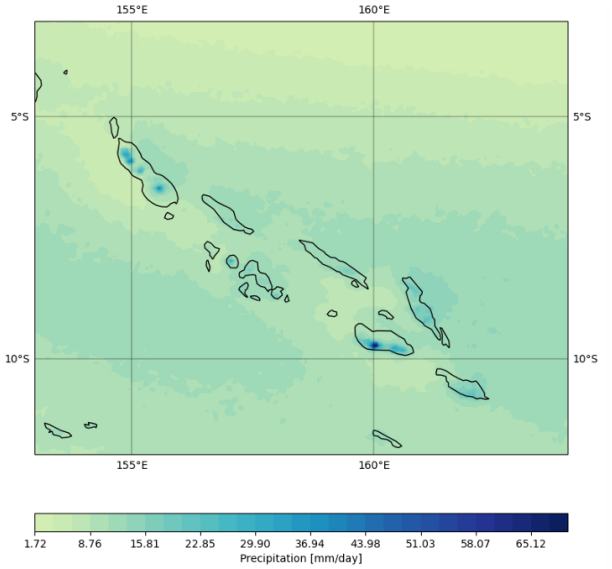

Figure 5.1: Zoom on the Solomon Islands showing climatology daily precipitation from ICON data for the 1990–2039 period.

Another observation, based on the standard deviation of the detrended time series, is that ICON exhibits stronger internal variability near the equator, particularly compared to ERA5, which may also indicate high variability in other regions of the world.

From the time series of the three cities, two unusual aspects can be observed when looking at maximum and minimum temperatures and their related indices. The first is that, in the early years, the values are higher than in the following years. This may be due to model drift,

which occurs when the initial conditions are inconsistent with the model dynamics, leading to one or two years of adjustment before the model becomes tuned (Manzanas, 2020). A second issue concerns the marked differences in the values of indices and temperatures before and after 2020. This arises because ICON uses two separate initial conditions: the historical simulation (1990–2020) and the future projection are not directly connected. The historical run is forced with observed boundary conditions, such as greenhouse gases and aerosols, to reproduce past variability and evaluate model performance. In contrast, the projection from 2020 onward is initialized independently using reanalysis data and a short ocean spin-up. This protocol introduces an artificial discontinuity around 2020, which should be understood as a methodological artifact rather than a real climate signal. Consequently, the focus should remain on long-term trends (ECMWF, 2025).

5.5 Possible Adaptation

This thesis shows that Climate change is expected to affect PICTs in a severe way, by enhancing the risk of floods and extreme precipitation, along with increases in both maximum and minimum temperatures, leading to more frequent heat waves.

The analysis shows that the different islands respond differently to climate change in terms of precipitation patterns, whereas temperature exhibits an increasing trend across the entire area. Additionally, the higher resolution allows for a more detailed examination of specific aspects.

Considering the whole area, plans for future flooding and extreme precipitations will be needed, while considering the droughts they should decrease, in concordance with the study conducted by Iese et al. (2021), in particular for the Fiji areas and cities like Suva. The analysis indicates that the main precipitation events will occur primarily over land rather than over the halo, posing a greater threat to the population.

Another major threat to the population is heat waves. They are expected to increase significantly over the halo, although a substantial rise is also projected over land and they have a directly impact on the human beings. Strengthening the health sector is essential to respond to prolonged periods of extreme heat and the deases that area lead with this increasing in temperature (Devadason, Jackson, and Cole, 2019). Urban planning could be highly beneficial for the PICTs, promoting active transportation and reforestation to help mitigate the urban heat island effect (Connell, 2023).

Due to their isolation, the adaptive capacity of small islands is very low, as they face a lack of

qualified personnel, high transportation costs, and limited access to information (Major et al., 2021).

Several projects are already underway to protect the small islands in the Pacific. One notable example is the Pacific Ecosystem-based Adaptation to Climate Change Plus (PEBACC+) Project, which operates in Fiji, New Caledonia, Solomon Islands, Vanuatu, and Wallis and Futuna. Its primary objective is to develop, sustain, and institutionalize ecosystem-based adaptation (EbA) and nature-based solutions (NbS) to climate change. The project also aims to strengthen regional cooperation among Pacific Island countries and territories. [1]

In order to strengthen the health system for the population, strategic frameworks like "The Western Pacific Framework for action on health and the environment," "Healthy Islands Vision," and "The SIDS Initiative" aim to provide national health authorities in SIDS with political, technical, and financial support to better understand and address the effects of climate change on health. Particular attention is needed for capacity development, surveillance and monitoring systems, as well as research to address priorities and translate findings into practice and policy (Bowen et al., 2024).

[1] https://www.sprep.org/pebacc-plus

6. Conclusions

Awareness and concern about climate change are increasing every day. Initiatives such as Destination Earth, which for the first time aims to develop a digital twin of the Earth using high-resolution models, are essential for enhancing our understanding of climate evolution over the coming decades and supporting adaptation efforts. The significant improvement in spatial resolution provides a particularly valuable resource for small islands, such as the PICTs, which are among the most vulnerable regions in the world (Bündnis Entwicklung Hilft and Institute for International Law of Peace and Armed Conflict, 2019).

As demonstrated by the results of this thesis, higher resolution allows the retrieval of information that would otherwise be lost in coarse-resolution models. Although this study focuses on only a small portion of the terrestrial surface, the impact of resolution is already evident when comparing the differing responses of the ocean, particularly the areas surrounding the islands, and the land to changes in model resolution. In particular, the case of the TN90p index highlights this effect: the analysis reveals that the warming trend is stronger over the halo region than over the islands, a distinction that was not captured in ERA5. Looking toward the near future under the plausible SSP3-7.0 scenario, temperatures are projected to continue rising, bringing with them severe and far-reaching consequences.

Global attention is needed for these territories to support them in facing the challenges they are already experiencing as a result of climate change. Although the ICON simulation still exhibits some issues, it also shows great potential for studying and understanding the complex region where these islands are located, demonstrating the important role of the Climate DT.

The results obtained in this thesis represent only a first step toward a better understanding of these complex and extremely important regions. Moreover, the analyses applied here could serve as a basis for similar studies on other small islands worldwide.

Bibliography

An, Soon-Il et al. (2012). "Recent and future sea surface temperature trends in tropical Pacific warm pool and cold tongue regions". In: *Climate dynamics* 39.6, pp. 1373–1383.

Aumann, Hartmut H, Steven Broberg, and Evan M Manning (2024). "Northward Shift and Narrowing of the ITCZ in 20 Years of AIRS Data". In: *Journal of Geophysical Research: Atmospheres* 129.5, e2023JD038723.

Australian Bureau of Meteorology (2024). *BARRA Dataset - OneClimate Portal*. Accessed on 28 July 2025. URL: https://oneclimate.acdguide.cloud.edu.au/records/3ap7t-a2842 (visited on 07/28/2025).

Barnett, Jon et al. (2025). "Migration as Adaptation? The Falepili Union Between Australia and Tuvalu". In: *Wiley Interdisciplinary Reviews: Climate Change* 16.1, e924.

Bauer, Peter (2022). *Forecasting the weather: A value chain from observations to applications*. Accessed: 31 July 2025. URL: https://www.ecmwf.int/en/newsletter/171/meteorology/forecasting-weather-value-chain-observations-applications.

Bourgault, Pascal et al. (2023). "xclim: xarray-based climate data analytics". In: *Journal of Open Source Software* 8.85, p. 5415. DOI: 10.21105/joss.05415. URL: https://doi.org/10.21105/joss.05415.

Bowen, Kathryn J et al. (2024). "Human health and climate change in the Pacific: a review of current knowledge". In: *Climate and Development* 16.2, pp. 119–133.

Brown, Josephine R et al. (2020). "South Pacific Convergence Zone dynamics, variability and impacts in a changing climate". In: *Nature Reviews Earth & Environment* 1.10, pp. 530–543.

Bündnis Entwicklung Hilft and Institute for International Law of Peace and Armed Conflict (2019). *World Risk Report 2019*. Accessed: 2025-07-25. Bündnis Entwicklung Hilft and Ruhr University Bochum. URL: https://weltrisikobericht.de/wp-content/uploads/2019/09/WorldRiskReport-2019_Online_english.pdf.

Bureau of Meteorology (2019). *BARRA Parameters Master List v1.0 – July 2019*. http://www.bom.gov.au/research/projects/reanalysis/BARRA_Parameters_Master_List_July_2019.v1.pdf. Accessed: 2025-07-28.

— (2021). *BARRA-R Product NCI Australia*. Dataset. DOI: 10.25914/6198bcb35c1c9. URL: https://dx.doi.org/10.25914/6198bcb35c1c9.

Cai, Ming (2003). "Formation of the cold tongue and ENSO in the equatorial Pacific basin". In: *Journal of climate* 16.1, pp. 144–155.

Chand, Savin et al. (2023). "Climate processes and drivers in the Pacific and global warming: a review for informing Pacific planning agencies". In: *Climatic Change* 176.2, p. 5.

Chen, Jie, François P Brissette, and Philippe Lucas-Picher (2015). "Assessing the limits of bias-correcting climate model outputs for climate change impact studies". In: *Journal of Geophysical Research: Atmospheres* 120.3, pp. 1123–1136.

Climate Change Adaptation Digital Twin (2024). https://destine.ecmwf.int/climate-change-adaptation-digital-twin-climate-dt/. Accessed: YYYY-MM-DD.

Climate Program Office, NOAA (Nov. 2024). *NOAA scientists host collaborative pre-proposal planning meetings for the Climate Variability and Predictability Program's FY25 Notice of Funding Opportunity*. https://cpo.noaa.gov/noaa-scientists-host-collaborative-pre-proposal-planning-meetings-for-the-climate-variability-and-predictability-programs-fy25-notice-of-funding-opportunity/. Accessed: 2025-09-16.

Climate.gov, NOAA (2021). *What are El Niño and La Niña?* Accessed: 2025-07-22. URL: https://www.climate.gov/news-features/understanding-climate/el-nino-and-la-nina.

Connell, John (2023). *Climate Change and Health: A Security Challenge in the Pacific Islands*.

Copernicus Climate Change Service (2017). *ERA5 hourly data on single levels from 1959 to present*. https://cds.climate.copernicus.eu/datasets/reanalysis-era5-single-levels?tab=overview. Accessed: 2025-07-28.

Cruz-González, Alejandro et al. (2025). "Climate change projections in temperature and precipitation using cmip6 in Central Mexico". In: *Theoretical and Applied Climatology* 156.2, p. 97.

Deo, Anil et al. (2021). "Tropical cyclone contribution to extreme rainfall over southwest Pacific Island nations". In: *Climate Dynamics* 56.11, pp. 3967–3993.

DestinE Project (2025). *Destination Earth*. https://destination-earth.eu/. Accessed: 12 September 2025.

Deutscher Wetterdienst (2024). *ICON Tutorial 2024*. https://www.dwd.de/DE/leistungen/nwv_icon_tutorial/pdf_einzelbaende/icon_tutorial2024.pdf. Accessed: 2025-07-31.

Devadason, CAROLINE ANITHA, LUKE Jackson, and JENNIFER Cole (2019). *Pacific island countries: An early warning of climate change impacts*.

Developers, SciPy (2025). *scipy.stats.mstats.linregress*. https://docs.scipy.org/doc/scipy/reference/generated/scipy.stats.mstats.linregress.html. Accessed: 2025-08-06.

Dhage, Laxmikant and Matthew J Widlansky (2022). "Assessment of 21st century changing sea surface temperature, rainfall, and sea surface height patterns in the tropical Pacific Islands using CMIP6 greenhouse warming projections". In: *Earth's Future* 10.4, e2021EF002524.

Doblas-Reyes, Francisco J et al. (2025). "The Destination Earth digital twin for climate change adaptation". In: *EGUsphere* 2025, pp. 1–41.

Doorga, Jay Rovisham Singh (2022). "Climate change and the fate of small islands: The case of Mauritius". In: *Environmental Science & Policy* 136, pp. 282–290.

ECMWF (2021). *The family of ERA5 datasets*. https://confluence.ecmwf.int/display/CKB/The+family+of+ERA5+datasets. Accessed: 2025-07-28.

— (2023). *ERA5: Data documentation*. Available at: https://confluence.ecmwf.int/display/CKB/ERA5%3A+data+documentation?src=spaceshortcut. Accessed: 28 July 2025.

— (2025). *Climate Change Adaptation Digital Twin (Climate DT) – Models*. https://destine.ecmwf.int/climate-change-adaptation-digital-twin-climate-dt/#models. Accessed on September 30, 2025.

European Centre for Medium-Range Weather Forecasts (ECMWF) (2025). *ECMWF – European Centre for Medium-Range Weather Forecasts*. https://www.ecmwf.int/. Accessed: 28 July 2025.

Fernández-Duque, B et al. (2024). "Changes in daily precipitation extremes over the Fiji Islands (1905–2021)". In: *Stochastic Environmental Research and Risk Assessment*, pp. 1–18.

Fiedler, Paul C (2002). "Environmental change in the eastern tropical Pacific Ocean: review of ENSO and decadal variability". In: *Marine Ecology Progress Series* 244, pp. 265–283.

Goldberg, Walter M. (2018). "An Introduction to the Tropical Pacific and Types of Pacific Islands". In: *The Geography, Nature and History of the Tropical Pacific and its Islands*. Cham: Springer International Publishing, pp. 1–38. ISBN: 978-3-319-69532-7. DOI: 10.1007/978-3-319-69532-7_1. URL: https://doi.org/10.1007/978-3-319-69532-7_1.

Grundner, Arthur et al. (2022). "Deep learning based cloud cover parameterization for ICON". In: *Journal of Advances in Modeling Earth Systems* 14.12, e2021MS002959.

Heim Jr, Richard R (2015). "An overview of weather and climate extremes–Products and trends". In: *Weather and Climate Extremes* 10, pp. 1–9.

Hersbach, H. et al. (2023). *ERA5 hourly data on single levels from 1940 to present*. Accessed on 09-Sep-2025. Copernicus Climate Change Service (C3S) Climate Data Store (CDS). DOI: 10.24381/cds.adbb2d47.

Hoffmann, Jörn et al. (2023). *Destination Earth–A digital twin in support of climate services*.

Holt, Charles A and Sean P Sullivan (2023). "Permutation tests for experimental data". In: *Experimental economics* 26.4, pp. 775–812.

Hoyer, S. and J. Hamman (2017). "xarray: N-D labeled arrays and datasets in Python". In: *Journal of Open Research Software* 5.1. DOI: 10.5334/jors.148. URL: http://doi.org/10.5334/jors.148.

Iese, Viliamu et al. (2021). "Historical and future drought impacts in the Pacific islands and atolls". In: *Climatic Change* 166.1, p. 19.

IPCC (2012). *Managing the Risks of Extreme Events and Disasters to Advance Climate Change Adaptation*. Ed. by C. B. Field et al. Special Report of Working Groups I and II of the Intergovernmental Panel on Climate Change. Cambridge, UK and New York, NY, USA: Cambridge University Press. URL: https://www.ipcc.ch/site/assets/uploads/2018/03/SREX_Full_Report-1.pdf.

Johnson, G. C et al. (2023). "Global Oceans". In: *Bulletin of the American Meteorological Society* 104.9, S146–S206. DOI: 10.1175/BAMS-D-23-0076.2. URL: https://journals.ametsoc.org/view/journals/bams/104/9/BAMS-D-23-0076.2.xml.

Jones, Philip W (1999). "First-and second-order conservative remapping schemes for grids in spherical coordinates". In: *Monthly Weather Review* 127.9, pp. 2204–2210.

Jupiter, Stacy, Sangeeta Mangubhai, and Richard T Kingsford (2014). "Conservation of biodiversity in the Pacific Islands of Oceania: challenges and opportunities". In: *Pacific Conservation Biology* 20.2, pp. 206–220.

Klein Tank, AMG and GP Können (2003). "Trends in indices of daily temperature and precipitation extremes in Europe, 1946–99". In: *Journal of climate* 16.22, pp. 3665–3680.

Kuleshov, Yuriy et al. (2014). "Extreme weather and climate events and their impacts on island countries in the Western Pacific: cyclones, floods and droughts". In: *Atmospheric and Climate Sciences* 4.5, pp. 803–818.

Linsley, Braddock K et al. (2017). "Abrupt northward shift of SPCZ position in the late-1920s indicates coordinated Atlantic and Pacific ITCZ change". In: *Past Global Changes Magazine* 25.1, pp. 52–56.

Liu, Wei et al. (2024). "Contrasting fast and slow intertropical convergence zone migrations linked to delayed Southern Ocean warming". In: *Nature Climate Change* 14.7, pp. 732–739.

Lo, YT Eunice et al. (2024). "Heat impacts on human health in the Western Pacific Region: an umbrella review". In: *The Lancet Regional Health–Western Pacific* 42.

Lv, Pengfei, Hongfei Hao, and Guocan Wu (2023). "Differences in global precipitation regimes between land and ocean areas based on the gpm imerg product". In: *Remote Sensing* 15.17, p. 4179.

Major, David C et al. (2021). "Adaptation to climate change in small island settlements". In: *Ocean & Coastal Management* 212, p. 105789.

Manzanas, Rodrigo (2020). "Assessment of model drifts in seasonal forecasting: sensitivity to ensemble size and implications for bias correction". In: *Journal of Advances in Modeling Earth Systems* 12.3, e2019MS001751.

McGree, Simon, Nicholas Herold, et al. (2019). "Recent changes in mean and extreme temperature and precipitation in the Western Pacific Islands". In: *Journal of Climate* 32.16, pp. 4919–4941.

McGree, Simon, Sergei Schreider, and Yuriy Kuleshov (2016). "Trends and variability in droughts in the Pacific Islands and Northeast Australia". In: *Journal of Climate* 29.23, pp. 8377–8397.

McIver, Lachlan et al. (2016). "Health impacts of climate change in Pacific Island countries: a regional assessment of vulnerabilities and adaptation priorities". In: *Environmental health perspectives* 124.11, pp. 1707–1714.

McNamara, Karen E et al. (2021). "Understanding and responding to climate-driven non-economic loss and damage in the Pacific Islands". In: *Climate Risk Management* 33, p. 100336.

Mearns, LO et al. (1995). "Analysis of daily variability of precipitation in a nested regional climate model: comparison with observations and doubled CO2 results". In: *Global and Planetary Change* 10.1-4, pp. 55–78.

Merkenschlager, Christian et al. (2021). "Assessing local daily temperatures by means of novel analog approaches: a case study based on the city of Augsburg, Germany". In: *Theoretical and Applied Climatology* 145.1, pp. 31–46.

Narsey, Sugata et al. (2022). "Storylines of South Pacific Convergence Zone changes in a warmer world". In: *Journal of Climate* 35.20, pp. 6549–6567.

NOAA National Climatic Data Center (2012). *Part 8. Climate of the Pacific Islands*. Tech. rep. NOAA Technical Report NESDIS 142-8. Accessed on [Inserisci data di accesso, es. July 5, 2025]. National Oceanic and Atmospheric Administration (NOAA). URL: `https://repository.library.noaa.gov/view/noaa/56815/noaa_56815_DS1.pdf`.

Nunn, Patrick D et al. (2016). "Classifying pacific islands". In: *Geoscience Letters* 3, pp. 1–19.

Nurisso, Matteo et al. (2025). *AQUA*. DOI: 10.5281/ZENODO.14906075. URL: https://zenodo.org/doi/10.5281/zenodo.14906075.

Pacific-Australia Climate Change Science and Adaptation Planning Program (2013). "Climate of the Western Tropical Pacific and East Timor". In: *Climate Variability, Extremes and Change in the Western Tropical Pacific: New Science and Updated Country Reports*. Australian Bureau of Meteorology and CSIRO, pp. 15–50. URL: https://www.pacificclimatechangescience.org/wp-content/uploads/2013/08/Ch.-2.-Climate-of-the-Western-Tropical-Pacific-and-East-Timor.pdf.

Palanivel, Hemalatha and Shipra Shah (2021). "Unlocking the inherent potential of plant genetic resources: food security and climate adaptation strategy in Fiji and the Pacific". In: *Environment, development and sustainability* 23.10, pp. 14264–14323.

Perkins, SE et al. (2007). "Evaluation of the AR4 climate models' simulated daily maximum temperature, minimum temperature, and precipitation over Australia using probability density functions". In: *Journal of climate* 20.17, pp. 4356–4376.

Riahi, Keywan et al. (2017). "The Shared Socioeconomic Pathways and their energy, land use, and greenhouse gas emissions implications: An overview". In: *Global Environmental Change* 42, pp. 153–168. ISSN: 0959-3780. DOI: https://doi.org/10.1016/j.gloenvcha.2016.05.009. URL: https://www.sciencedirect.com/science/article/pii/S0959378016300681.

Robeson, Scott M (2002). "Relationships between mean and standard deviation of air temperature: Implications for global warming". In: *Climate Research* 22.3, pp. 205–213.

Schulzweida, Uwe (n.d.). *CDO User Guide — First Order Conservative Remapping (REMAPCON)*. https://code.mpimet.mpg.de/projects/cdo/embedded/index.html#XYAC. Accessed: 2025-09-15.

Schwarzwald, Kevin et al. (2021). "Changes in future precipitation mean and variability across scales". In: *Journal of Climate* 34.7, pp. 2741–2758.

Seager, Richard, Naomi Henderson, and Mark Cane (2022). "Persistent discrepancies between observed and modeled trends in the tropical Pacific Ocean". In: *Journal of Climate* 35.14, pp. 4571–4584.

Shah, Shipra, Asinate Moroca, and Jahangeer A Bhat (2018). "Neo-traditional approaches for ensuring food security in Fiji Islands". In: *Environmental development* 28, pp. 83–100.

Su, C.-H. et al. (2019). "BARRA v1.0: the Bureau of Meteorology Atmospheric high-resolution Regional Reanalysis for Australia". In: *Geoscientific Model Development* 12, pp. 2049–2068. DOI: 10.5194/gmd-12-2049-2019. URL: https://doi.org/10.5194/gmd-12-2049-2019.

Taylor, Subhashni (2021). "The vulnerability of health infrastructure to the impacts of climate change and sea level rise in small island countries in the South Pacific". In: *Health Services Insights* 14, p. 11786329211020857.

The World Bank (n.d.). *Solomon Islands — Climate Data (Historical)*. `https://climateknowledgeportal.worldbank.org/country/solomon-islands/climate-data-historical`. Accessed: 2025-09-15.

Waskom, Michael (2024). *Visualizing statistical relationships — Seaborn: Statistical Data Visualization*. Accessed: 2025-08-08. URL: `https://seaborn.pydata.org/tutorial/distributions.html#tutorial-kde`.

Waskom, Michael L. (2021). "seaborn: statistical data visualization". In: *Journal of Open Source Software* 6.60, p. 3021. DOI: `10.21105/joss.03021`. URL: `https://doi.org/10.21105/joss.03021`.

Widlansky, Matthew J et al. (2013). "Changes in South Pacific rainfall bands in a warming climate". In: *Nature climate change* 3.4, pp. 417–423.

Wimhurst, Joshua J and J Scott Greene (2021). "Updated analysis of gauge-based rainfall patterns over the western tropical Pacific Ocean". In: *Weather and Climate Extremes* 32, p. 100319.

Wolf, Franziska et al. (2021). "Influences of climate change on tourism development in small pacific island states". In: *Sustainability* 13.8, p. 4223.

World Meteorological Organization (2024). *State of the Climate in the South-West Pacific 2023*. Tech. rep. WMO-No. 1356. Accessed: 2025-09-08. World Meteorological Organization. URL: `https://library.wmo.int/viewer/68995/download?file=1356_State-of-the-Climate-in-SWP-2023_en.pdf&type=pdf&navigator=1`.

— (2025a). *State of the Climate in the South-West Pacific 2024*. Accessed: 2025-07-22. URL: `https://library.wmo.int/viewer/69552/download?file=1356_State-of-the-Climate-in-SWP-2024_en.pdf&type=pdf&navigator=1`.

— (Mar. 2025b). *State of the Global Climate 2024*. WMO-No. 1368. Geneva, Switzerland: World Meteorological Organization. URL: `https://wmo.int/sites/default/files/2025-03/WMO-1368-2024_en.pdf`.

Zelle, Hein et al. (2004). "The relationship between sea surface temperature and thermocline depth in the eastern equatorial Pacific". In: *Journal of physical oceanography* 34.3, pp. 643–655.

Zhang, Xuebin et al. (2011). "Indices for monitoring changes in extremes based on daily temperature and precipitation data". In: *Wiley Interdisciplinary Reviews: Climate Change* 2.6, pp. 851–870.

A. Appendix: Climatology and Detrending of Daily Maximum and Minimum Temperatures from ERA5, BARRA, and ICON (1990–2019)

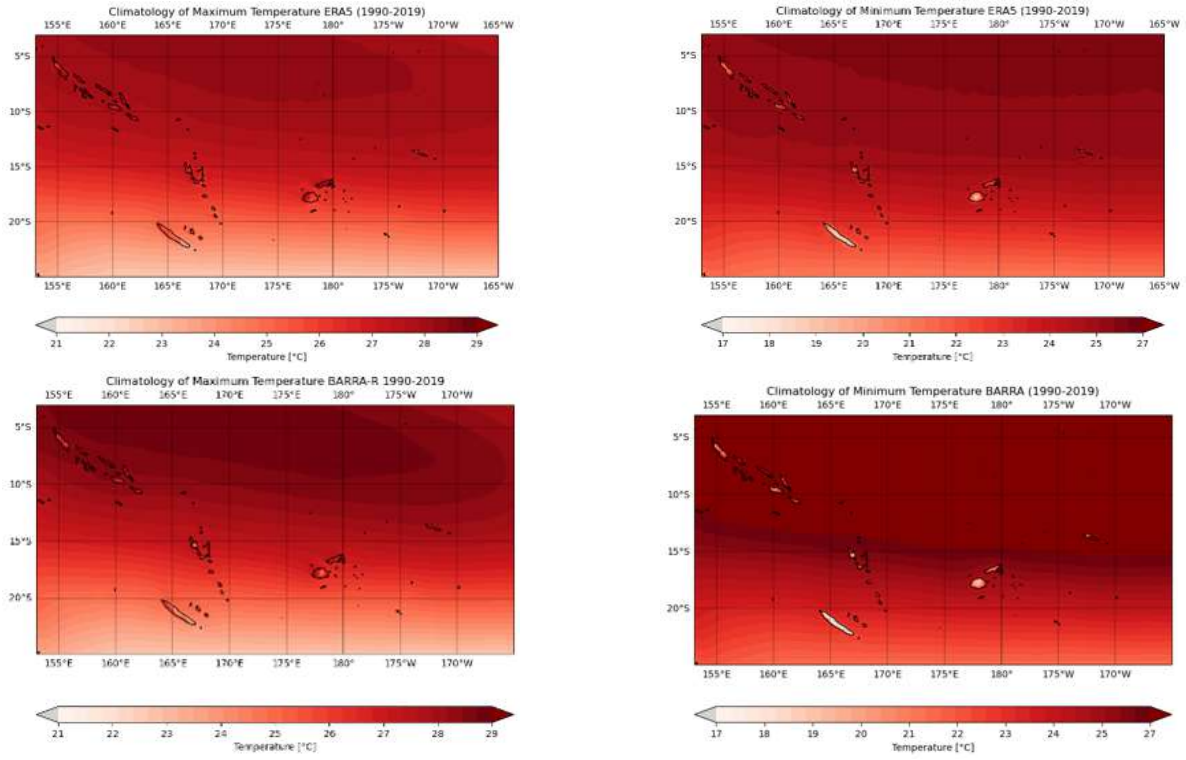

Figure A.1: Climatology of Daily maximum (Tmax on the left) and minimum (Tmin on the right) temperatures for 1990–2019 over the area of interest, based on ERA5 (top) and BARRA (bottom). Pixels with Tmax > 29 °C or Tmin > 27 °C are shown in dark red, while those with Tmax < 21 °C or Tmin < 17 °C are shown in light grey.

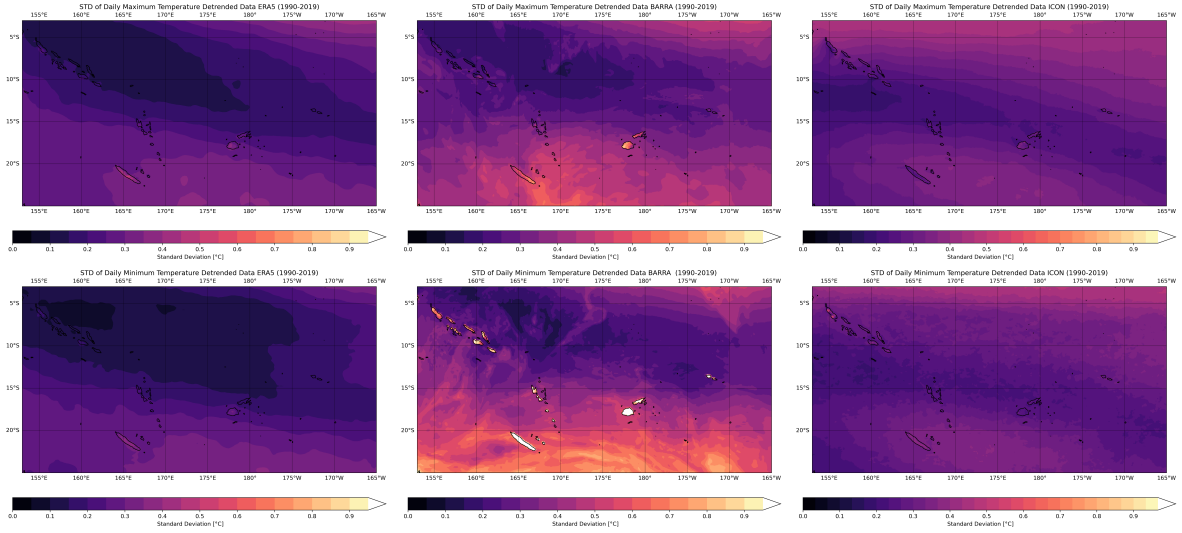

Figure A.2: Daily Maximum (top) and Minimum (bottom) Temperature standard deviation after detrending for ERA5, BARRA, and ICON (from left to right) (1990–2019). Standard deviation values above 0.9°C are marked in white.

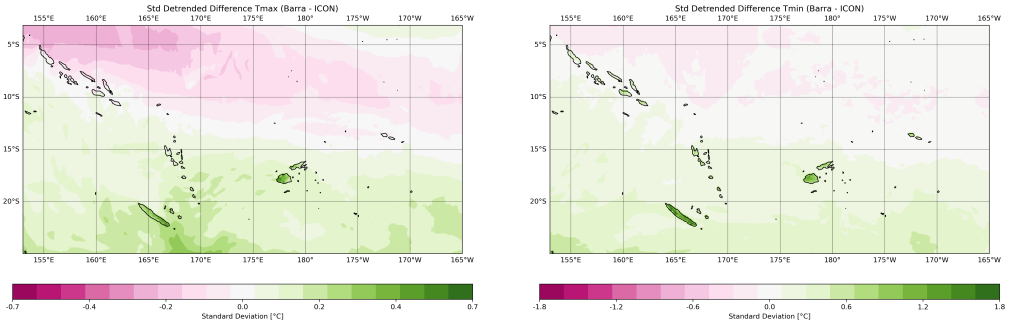

Figure A.3: Difference between BARRA and ICON standard deviations, shown in Figure A.2, for the period 1990–2019.

B. Appendix: Trends of the ETCCDI indices (1990-2019) and (1990-2039)

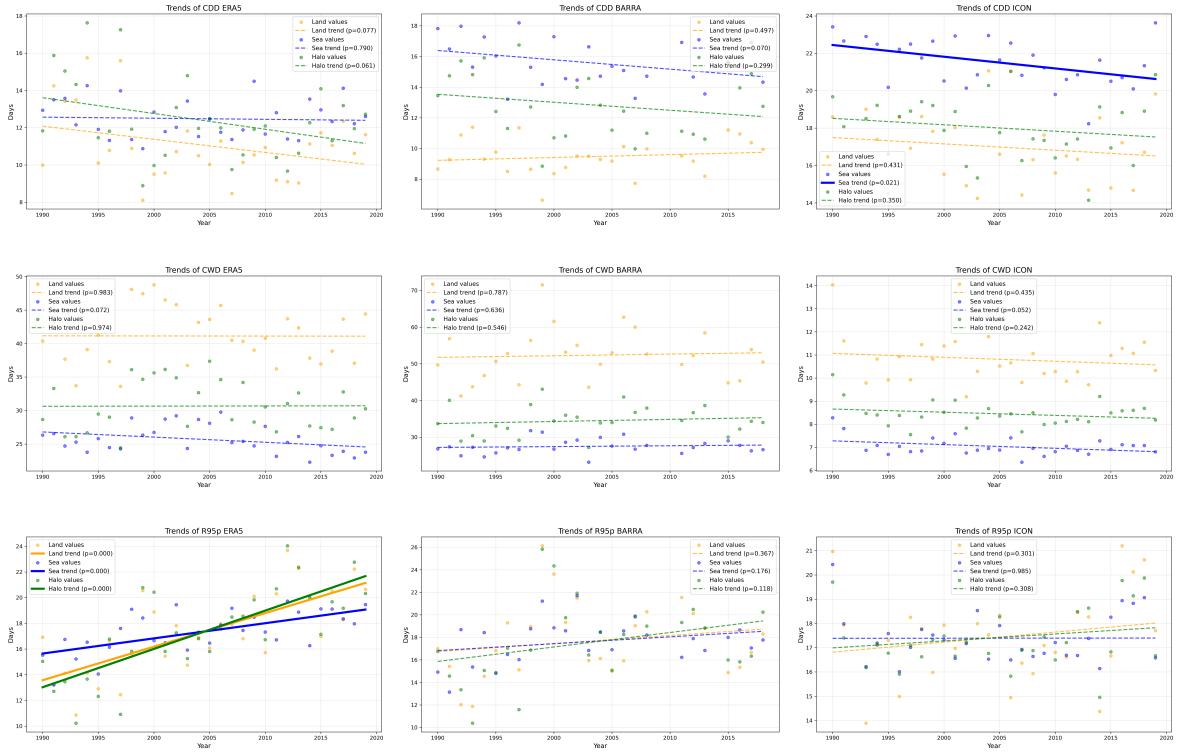

Figure B.1: Trends of the first three ETCCDI indices (CDD, CWD, R95p), shown row by row, for ERA5, BARRA, and ICON (from left to right) (1990-2019). A continuous line indicates a statistically significant trend ($p < 0.05$), while a dashed line indicates a non-significant trend.

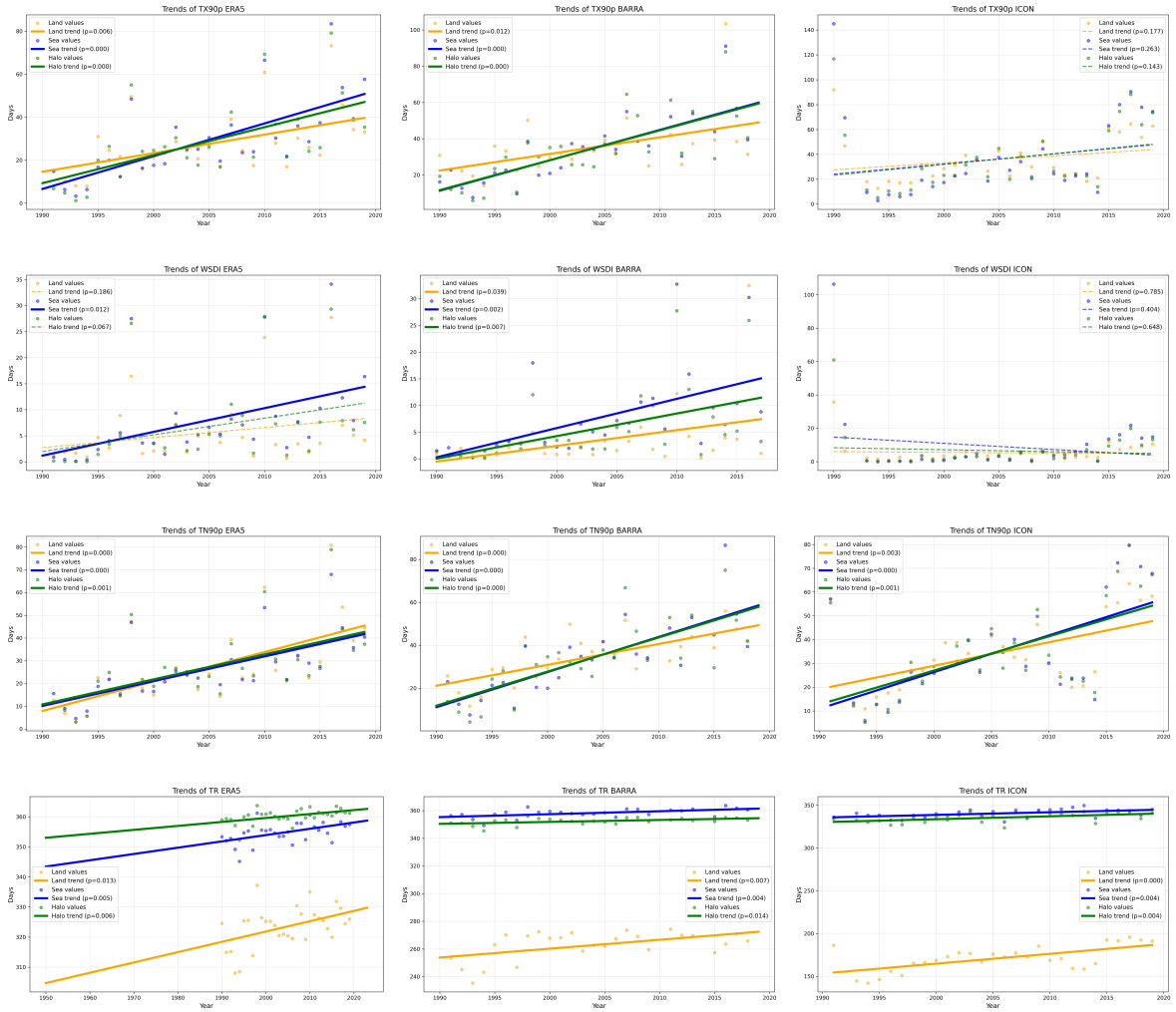

Figure B.2: Trends of the last four ETCCDI indices (TX90p, WSDI, TN90p, TR), shown row by row, for ERA5, BARRA, and ICON (from left to right) (1990-2019). A continuous line indicates a statistically significant trend ($p < 0.05$), while a dashed line indicates a non-significant trend.

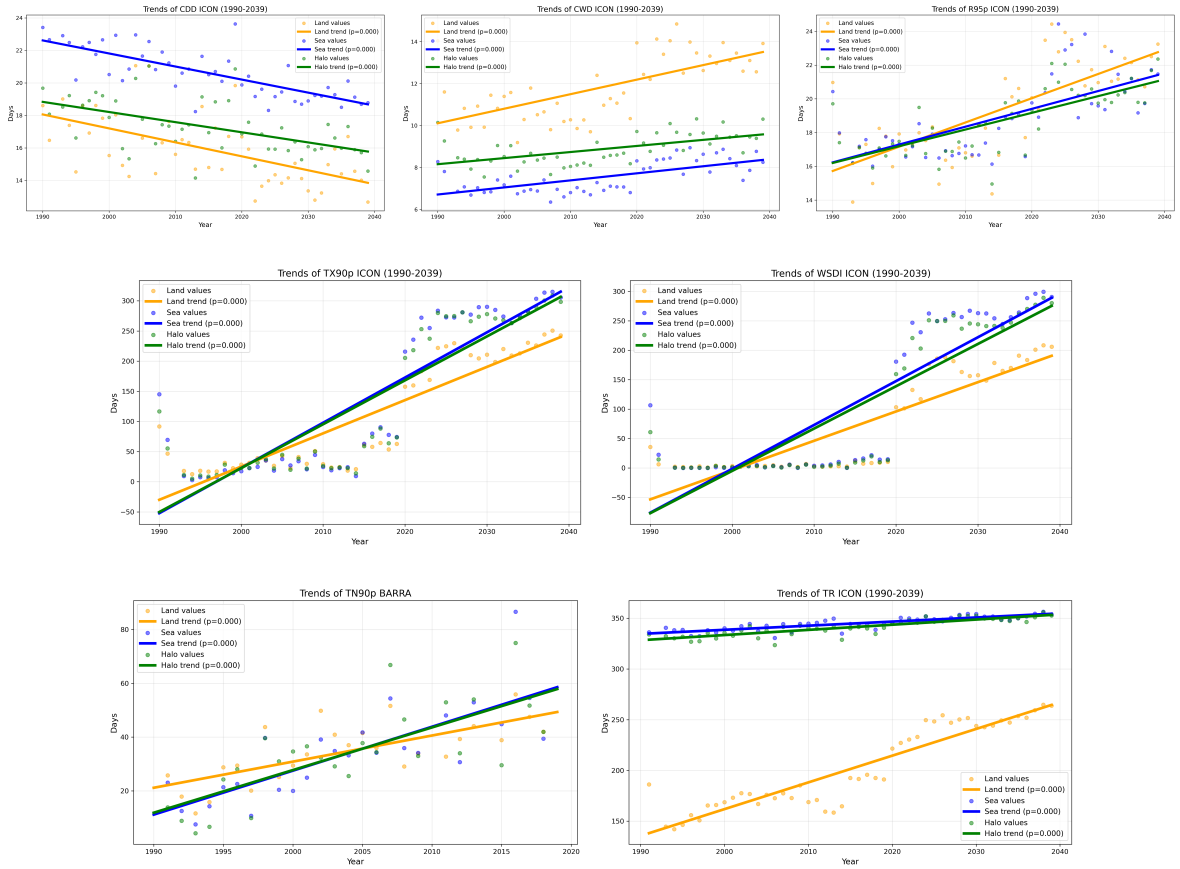

Figure B.3: Trends of the seven ETCCDI indices (CDD, CWD, R95p, TX90p, WSDI, TN90p, TR), shown row by row, for ICON (1990-2039). A continuous line indicates a statistically significant trend ($p < 0.05$), while a dashed line indicates a non-significant trend.